

**Enhanced Rock Weathering in Agricultural Settings:
Field Trial at Zumwalt Acres in Sheldon, IL**

Gavrielle Welbel

In partial fulfillment of the requirements of the bachelors of science degree in Earth & Planetary
Science at Yale University

Advisor: Noah Planavsky
Second Reader: Lidya Tarhan

Acknowledgements

The work presented in this report is the result of collaboration between a tremendous team of researchers in the Earth and Planetary Science department at Yale University, the Yale School of the Environment, and Georgia Technological Institute, along with farmers and apprentices at Zumwalt Acres. This research would not have been possible without the labor, insight, and commitment of countless people on the ground in Sheldon, and in the laboratory.

I would like to thank Noah Planavsky for enabling and guiding this research over the past three years, as well Chris Reinhard for his input and support. Tom Reershemius has played a key role in the development and deployment of this field trial, in analyzing results, and in thinking through implications of this work. Tom, Marya Matlin-Wainer, Isabelle Davis, Rocco D'Ascanio, Borianna Calderon-Asael, and Maddie Bartels, with support from Dan Asael, conducted the laboratory analysis that is foundational to this work. Jake Jordan supported data processing and analysis. Sophie Lieberman, Lexi Weintraub, Evelin Pilhap, and Mark Bradford supported experimental design. Sophie, Lexi, Marya, Isabelle and I along with many Zumwalt Acres apprentices conducted soil sampling and analysis on the ground and helped facilitate basalt deployment over the past three years. I am grateful to the entire Zumwalt Acres team for their enthusiasm about enhanced rock weathering, willingness to help in countless ways (especially Joey Finnegan, Tuomas Sivula, Sophie Johnson, Eric Luu, Patricia Mathu, Lilly Witonsky, Hannah Kahn Glass, Remi Welbel), and commitment to thinking through the complex scientific and societal quandaries of a just ERW roll-out.

John, JR, and Mark Zumwalt farm the land where these trials are based, and they played an essential role in this research. As early adopters, they allowed a novel approach to be implemented, and then accommodated the research needs, and patiently addressed questions about site history, management, and experience.

The location of the field study, colonially known as Sheldon, IL, is the homeland of the Kikapoo, Peoria, Miami, Kaskaskia, and Ocethi Sakowin peoples. It is in part due to generations of their stewardship that we have rich soil to farm today.

Table of Contents

ABSTRACT	6
INTRODUCTION	6
SECTION 1: FIELD SITE DESCRIPTION	9
ZUMWALT ACRES	9
TEST SITES	9
SITE #1	11
SITE #2	12
SITE #3	12
SITE #4	13
SITE #5	14
SOIL COMPOSITION IN SITE #1	14
MANAGEMENT	15
SITE #1	15
SITE #2	16
SITE #3	16
SITE #4	16
SITE #5	16
SOURCING FEEDSTOCK	16
TRANSPORTATION	17
SPREADING	17
SAMPLING	17
SITE #1	17
SITE #2 AND #3	17
SITE #4	18
SITE #5 AND #6	18
SECTION 2: SOIL PH	19
METHODS	19
ON-SITE: SOIL-WATER SLURRY PH	19
ON-SITE: CaCl ₂ SOLUTION PH	19
LABORATORY: SOIL-WATER SLURRY	19
LABORATORY: SIKORA BUFFER PH	20
RESULTS	20
SPATIAL VARIABILITY	20
TEMPORAL VARIABILITY	22
STATISTICAL ANALYSIS	23
DISCUSSION	24

SECTION 2: YIELDS	26
METHODS	26
SITE #1	26
SITES #2 AND #3	26
SITE #4	26
SITE #5	26
SITE #6	26
RESULTS	26
DISCUSSION	28
SITE #1	28
SITE #5 AND #6	28
SECTION 3: TICAT	30
METHODS	30
EXTRACTING EXCHANGEABLE CATIONS	30
TOTAL ACID DIGEST	30
ISOTOPE SPIKE COCKTAIL	30
ELEMENTAL ANALYSIS	31
TICAT FRAMEWORK: SOLID SAMPLE MASS BALANCE APPROACH	31
RESULTS	34
TI AND CATION CONCENTRATIONS ACROSS INDIVIDUAL SAMPLE POINTS	34
CATION DISSOLUTION AND CATION LOSS	41
CARBON DIOXIDE REMOVAL	44
DISCUSSION	45
TITANIUM	45
CATIONS	45
REDESIGNED SAMPLING PLAN TO CAPTURE SIGNAL FROM ERW	46
CARBON DIOXIDE REMOVAL	47
SECTION 4: CARBON BUDGET	51
METHODS	51
CARBON CYCLE	51
SOIL STOCK	51
GPP AND ECOSYSTEM RESPIRATION	52
HARVEST	52
ADDITIONAL INPUTS	52
OVERALL	52
BASALT INPUTS	52
BASALT CARBON CAPTURE	53
DISCUSSION	53
CONCLUSION	56

OTHER CONSIDERATIONS	56
NEXT STEPS	57
SAMPLING	57
SOIL HEALTH	57
LOOKING FORWARD: DEPLOYMENT	58
REFERENCES	60
<hr/>	
APPENDIX	66
<hr/>	
ADDITIONAL SAMPLING NOT REPORTED	66
GEOLOGICAL HISTORY OF THE REGION	66
COLONIAL HISTORY OF THE REGION	67
CARBON BUDGET	68
PIONEER VALLEY BASALT PARTICLE SIZE AND MINERALOGY	70

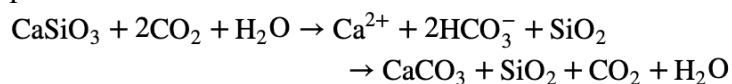
Abstract

A longitudinal study on the effects and implications of agricultural enhanced rock weathering (ERW) in the American Midwest is in its third year of study. ERW is the process of spreading crushed rocks on land with the intention of speeding up the natural process of rock weathering to capture atmospheric carbon dioxide (CO₂). Agricultural ERW has significant potential to capture atmospheric carbon dioxide, benefit farmers, and repurpose a mining by-product that is otherwise considered waste. However, the effects of ERW on greenhouse gas emissions and ecosystem health are still not well understood, especially at the scale of ERW deployment that is suggested. At Zumwalt Acres, in Sheldon, Illinois, the most robust study on ERW in active farmland to date is investigating basalt deployment in corn, soy, and hay fields, and cow pasture. Focusing on results from the 2022 growing season, soil pH was not significantly altered, although it began at close to neutral. Soy and corn yields remained relatively consistent, while hay and oat yields increased substantially with basalt application. Approximately 3.5 tons of carbon dioxide per hectare are estimated to have been captured six months after basalt treatment, however, the data was insufficient to confidently quantify carbon dioxide removal. This study provides key insights into data collection and analysis that should be conducted in field trials going forward to better understand and define the appropriate scope of enhanced rock weathering in agricultural settings as a negative emissions technology, and as one component in a larger shift of large-scale agriculture in the American Midwest to increase environmental and economic resiliency. At scale, rock weathering could capture gigatons of carbon dioxide, meanwhile improving crop yields and soil health, but the full scope of implications must be better understood before rolling out deployment across the country, and around the world.

Introduction

Enhanced rock weathering is a promising technology for vast removal of atmospheric carbon dioxide in order to mitigate the worst effects of climate change. The process of enhanced silicate weathering includes adding crushed silicate-based-rock (e.g., basalt) on land to capture CO₂ from the atmosphere and transport it as bicarbonate for permanent storage in oceans, thereby reducing ocean acidification.

Rock weathering occurs naturally all over earth's surface as rocks dissolve in water and react with acid. Compounds in the rock separate into ions, react with carbonic acid that came from CO₂ in the atmosphere, and then form solid calcium carbonate. This reaction is governed by the Urey equation:



Rock weathering is a negative feedback loop, moderating earth's temperature. When the earth warms, rock weathering occurs at greater speeds, capturing CO₂ from the atmosphere and cooling the planet (Brantley et al. 2023). However, at the current rate of anthropogenic carbon dioxide emissions, natural sinks cannot keep up.

Terrestrial ERW speeds up this natural process by utilizing rock with a high surface area and fast-weathering minerals, and applying it to warm, moist land where it will be exposed to carbonic acid. Agricultural fields are a prime location for enhanced rock weathering because they are large flat surfaces that experience significant precipitation and can benefit from the rock as a fertilizer. Farmers in the Midwest are accustomed to spreading crushed limestone on their fields every four years to neutralize soil pH, so the infrastructure for spreading rock dust is generally available.

ERW is suggested to neutralize soil pH, increase crop yields, introduce macro and micronutrients, reduce heavy metal uptake by plants, and mitigate N₂O emissions. Hypothetical models indicate huge potential for carbon capture, but large-scale field-based studies must be conducted to understand outcomes of enhanced rock weathering under real-world conditions.

Ongoing field-based research trials on agricultural ERW are being conducted by the Leverhulme Center for Climate Change Mitigation (LC3M) based out of University of Sheffield, The Working Lands Center based out of University of California Davis, University of Copenhagen in Denmark, and University of Guelph in Ontario, Canada. LC3M has trials around the world including at University of Illinois in Champaign Urbana, Sabah, Malaysia, North Wyke, UK, and Harpenden, UK.

Still, to date, very limited empirical data on carbon capture, soil health, and crop yields has been published based on farm-scale research (Almaraz, 2022; Haque 2020; Taylor 2021; Larkin 2022). Mechanistic models have been used to predict the outcomes of ERW in agricultural settings (Taylor 2017; Beerling 2020; Kanzaki 2022). Laboratory and mesocosm experiments have also our increased understanding of feedstock dissolution, and of plant nutrient uptake (Amann 2020; Kelland 2020; Dietzen 2018; Renforth 2015; Pogge von Strandmann 2021; Jariwala 2022,;Vienne 2022). In general, these studies suggest that the potential for significant carbon drawdown is dependent on feedstock mineralogy and particle size, soil properties, tillage, irrigation, and temperature (see table 9 in section 3 for CDR reported in the literature). Studies also suggest co-benefits including increased plant nutrient uptake and crop yields (Beerling 2020). Initial models and mesocosm studies also indicate reductions in N₂O emissions, a potent greenhouse gas, as a result of ERW deployment (Val Martin 2023; Chiaravalloti in-review).

These modeling, laboratory, and mesocosm studies suggest that applying basalt and other silicate-rocks to farms will have positive impacts for farmers, ecosystems, and climate change mitigation, with few negative consequences. Still, field data from working farms is necessary to understand how hypothetical predictions map onto real-world experience. Due to high variability in environmental conditions, land management, and deployment regimes in current and future ERW sites and within a site, a monitoring, reporting, and verification (MRV) framework is necessary to understand carbon capture in each deployment. Moreover, ERW impacts on soil and plant health can only be well understood in a field setting. Empirical data from field studies will both verify model, laboratory, and mesocosm studies and inform our understanding of the extent of variation across the ERW deployment landscape.

Most studies to date have been on university-run farms (e.g. University of Illinois Energy Farm, University of California Davis Working Lands Innovation Center). Working on university farms

has the benefit of more closely controlled conditions, access to specialized equipment, and freedom to experiment without fear of risking a farmer's bottom-line. By conducting field trials on working farms, managed by active farmers, on the other hand, the challenges and opportunities of deployment under real world conditions become apparent. To develop robust MRV frameworks, it is crucial to consider the variability in conditions (e.g. changes in management practices from year-to-year and unpredictable planting and harvest dates) that farmers experience, which is often not represented by highly controlled experimental plots on university farms. Working with active farmland illuminates the logistical challenges of sourcing, transporting, and spreading that farmers might encounter. Lastly, farmers are key players in the roll-out of ERW across the country, so it is crucial to have their input and buy-in throughout the research process. The field trials at Zumwalt Acres are among the largest and most geospatially robust field trials on active farmland to date.

In the next section, a description of the field site and deployment is described. In the following sections, the measured soil pH, titanium and cation concentrations, carbon dioxide removal, and crop yields in test plots treated with basalt, and as compared to control plots, is reported. Finally, considerations of the implications of this study and next steps are provided.

Section 1: Field Site Description

This study is based on farmland managed by Zumwalt Acres and neighboring farmers. The focus of this report is on one site of study within the larger field trial.

Zumwalt Acres

Zumwalt Acres is a community-led regenerative farm in Sheldon, IL (40.80, -87.5378). For the past 75 years, the land has been farmed in a conventional corn-soy rotation. The region is dominated by conventional agriculture, with 96% of land in the country dedicated to cropland (USDA 2017 Census of Agriculture). The approximate mean annual temperature is 12°C. The annual approximate rainfall is 850mm, making it a humid to wet climate. Three primary soil types are represented in our test plots, all of which are variations of loam soil. Experiments were done in collaboration with neighboring farmers (see www.zumwaltacres.org for more information).

Test Sites

Approximately 100 hectares are monitored currently to understand the multi-year impact of ERW on farms. In spring 2021, seven acres received basalt treatment, and corresponding control plots were established. In spring 2022, 21 hectares were treated with basalt. In 2023, two hectares will receive treatment, and in 2024, approximately 24 hectares are expected to have basalt applied. Site #1 is the focus of this report because it is the largest and most robust site that has received basalt application to date.

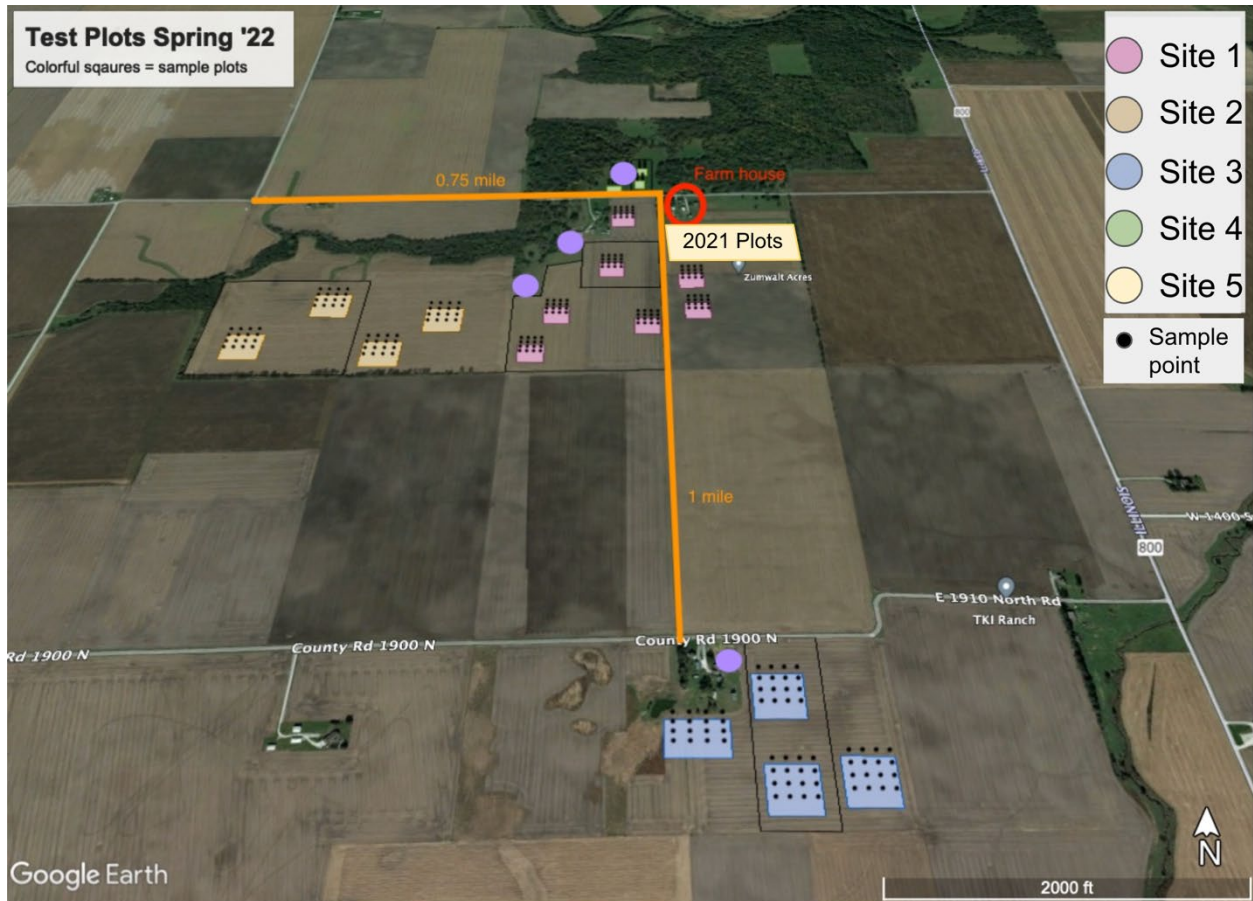


Figure 1: Map of all current test sites and sample locations. Pink, yellow, and blue squares indicate sample plots that range in size from 0.49ha to 1ha. Black boxes indicate zones where basalt has either already been applied or will receive application. Purple circles indicate where drainage water samples are collected from drainage tile outlets into a creek.

Figure 4: Map of Site #3, a conventional corn/soy field that has not yet received basalt application. Baselines soil samples are being collected. Basalt application is expected in fall 2023.

Site #4



Figure 5: Map of site #4, a cow pasture that received basalt application at a rate of 25 t/ha in April 2022.

Site #5



Figure 6: Map of Site #5, a hay field that received basalt application in April 2021 at varying rates, and site #6, a field with rotating crops that received basalt application in April 2021 at varying rates. The type of basalt applied is noted on the right of the image.

Soil composition in Site #1

	Slope (%)	Drainage	Runoff	Ksat (cm/hr)	Water Table (cm)	Flooding /Ponding	Available water supply, 0 - 152cm (cm)	Max CaCO ₃ content (%)	Restrictive feature (cm)
490A	0-2	Somewhat poorly drained	Low	0.5-1.5	30-60	None/None	19.6	40	> 200
102A	0-2	Somewhat poorly drained	Low	1.5 - 5	30-60	None/None	18.4	10	> 200

125A	0-2	Poorly drained	Negligible	1.5 - 5	0 - 30	None/Frequent	23.6	20	> 200
------	-----	----------------	------------	---------	--------	---------------	------	----	-------

Table 1: Characteristics of the three types of soils represented in Site #1 (USDA, Web Soil Survey)

	Layer	Depth (cm)	Soil Type
490A	1	0 - 28	Silt Loam
102A	1	0 - 41	Loam
125A	1	0 - 53	Loam
490A	2	28 - 66	Clay Loam
102A	2	41 - 81	Clay Loam
125A	2	53 - 117	Loam
490A	3	66 - 152	Loam
102A	3	81-122	Sandy Loam
125A	3	117 - 152	Stratified Loamy Sand to Silt Loam
102A	4	122 - 152	Stratified Loamy Sand to Silt Loam

Table #2: Depth profile of three types of soil represented in Site #1 (USDA, Web Soil Survey)

Management

Site #1

Date	Practice
Fall 2020	Limestone, diammonium phosphate, potash, ammonium sulfate applied
April 2021	Liquid N fertilizer + N stabilizer sprayed
May 2021	Field cultivated, corn planted <i>3 wks after planting</i> : liquid N fertilizer (side-dress) and herbicide applied
June 2021	Liquid herbicide applied
October 2021	Corn harvest
March 2022	Baseline soil samples
April 2022	Basalt applied, field cultivated Manure applied on sections of the field Soil samples
May 2022	Field cultivated, soy planted

June 2022	Liquid herbicide applied Soil samples
July 2022	Liquid herbicide applied
August 2022	Soil samples
September 2022	Bean harvest
October 2022	Soil samples
April 2023	Soil Samples Liquid N fertilizer + N stabilizer sprayed
May 2023	Field cultivated, corn planted

Table #3: On-farm practices between fall 2020 to May 2023

Site #2

Management at Site #2 is comparable to Site #1 but basalt has not been applied. Limestone was applied in fall 2022.

Site #3

Management at Site #2 is comparable to Site #1, but basalt has not been applied.

Site #4

Cows pasture on this site approximately 12 weeks out of the year in May, July, and September. It has been a pasture for at least 100 years, with a combination of bluegrass and brome.

Site #5

This 8-hectare field was converted from a conventional corn/soy field to an organic hay field in the spring of 2021. Oats, alfalfa, and timothy were planted on 4.9 hectares in 2021. Alfalfa and timothy are perennial grasses, while oats are annual. The oat seed and straw, and alfalfa and timothy hay were harvested in 2021. Alfalfa and timothy hay were harvested again in 2022. On the remaining 3.1 hectares, buckwheat was planted in spring 2022, and oats, alfalfa and timothy were planted in spring 2023.

Sourcing Feedstock

Numerous logistical constraints impede large-scale field experiments. First, a suitable feedstock must be identified. In the United States, the most accessible suitable feedstocks are basaltic. The feedstock must be low in heavy metals to avoid contamination and it should be fast weathering, to allow for carbon capture on reasonable timescales. Mining operations often have fine rock material as a byproduct that is sifted out from the usable material. Companies that produce roofing shingles are common miners of basalt in the U.S.

We worked with Specialty Granular (SGI), a roofing company with basalt mines in Hagerstown, MD, Blue Ridge Summit, PA, Waynesboro, PA, Pembine, WI, Annapolis, MO, and Ione, CA. We used basalt sourced from Blue Ridge Summit, PA from SGI in year one. In year one and in year two, we sourced basalt from Pioneer Valley, Ma, as it is igneous and faster weathering than the Blue Ridge metabasalt. Rock Dust Local supplied the Pioneer Valley basalt. Going forward, closer mine sites will be utilized to minimize transportation distance. On site 1, Pioneer Valley basalt was applied. The Pioneer Valley basalt that was used had 93.7% passing through a #30 mesh sieve. See appendix for more information minerology and particle size.

To date, SGI stores the fine basalt rock dust in a retired mine, filling it back up to ground level or above. The company then applies a few inches of topsoil, and plants grass. Instead, that rock dust could be spread on agricultural fields.

Transportation

To date, basalt has been transported in semi-trucks. Trucking is expensive from both an economic and emissions standpoint, but it is the only feasible option right now. Railways and barges are being explored for better transportation. As well, closer mine locations, in Wisconsin and Michigan, are being considered for Midwest deployment going forward.

Spreading

Standard agricultural lime spreaders can be used to spread the crushed basalt that we received. Full Throttle Ag Service based in Milford, Illinois was contracted (see www.longlivesoil.com for more information).

Sampling

Site #1

Each plot in Site #1 has been designed to have a 70m x 70m subplot in each soil type that is represented in the field, as shown in figure 2. The subplot is sampled in a grid of 16 samples, spaced equally. Each point is geolocated so that it can be returned to for subsequent sampling. A Garmin GPSMAP® 65s handheld GPS was used, which allows accuracy within 15 meters 95% of the time. Under normal conditions, accuracy generally improves to 3 to 5 meters, depending on the strength of the satellite signal.

In March before basalt application, all 16 points were sampled in each plot in each site using a 1" x 36" Hammer Head Replaceable Tip Soil Probe. In April 2022, basalt was applied to Sites 1 and 4.

In April, eight points were sampled in each plot in Site 1. Four points were sampled in each plot in Site 2, Site 3, and Site 4. In June, August, and October four samples, spaced throughout the grid, were sampled in Site 1. In July, four samples were taken in Site 4.

When samples were collected, one was collected down to 30cm, and split into three segments—0-10 cm, 10-20 cm, and 20-30 cm. Starting in the June sampling, a second sample was taken within approximately one meter radius from the first sample down to 10cm and combined with the other 0-10cm sample.

Site #2 and #3

The same sampling regime was used in site #2 and #3 and sampling occurred in March, April and August 2022. Sampling will occur again in May 2023. Baselines soil samples are being collected to monitor background variation in soil over time, which can be used to compare to variation in fields that received basalt treatment, and to be used as reference after basalt is applied to site #2 in the future.

Site #4

The same sampling regime was used in site #4 and sampling occurred in March, April, July, and October.

Site #5 and #6

In 2021, two soil samples were taken per plot at 0-10cm. One sample was taken on the east side and one on the west side of the field in approximately the same location each time. In 2022, the sampling protocol was adjusted to take samples of 0-30cm and 0-10cm in three locations in the field—east, west, and center.

Section 2: Soil pH

Methods

On-Site: Soil-Water Slurry pH

The soil pH was measured on samples taken from the top 0-10 cm. In April, pH was measured on eight samples in plots A and B, five samples in plot C, and four samples in plots D through S (all Site 1). In June, pH was measured in three samples in each plot A-S. In July, pH was measured on three samples from each plot in Site 4. In August, pH was measured in 16 samples in plots A and B, and 3 samples in plots C-F (all Site 1), as well as in three samples in each plot in Site 2 and Site 3.

Number of samples on which pH was taken varied to assess heterogeneity of pH across a plot, while minimizing number of samples needed.

The method to measure soil pH onsite is adapted from the Kellogg Soil Survey Laboratory Methods Manual (Soil Survey Staff 2022). The pH is measured in both soil-water (1:1) and soil-salt (1:2 CaCl₂) solutions. First, approximately 12g of each soil sample is measured into paper cups. Soil must air dry completely before measuring pH. This may take 2-4 days.

Once dried, each sample is crushed using a clean utensil. Into a new labeled cup, exactly 10g of dried soil is measured. Then, 10 mL of deionized (DI) water is added to 10g of soil (1:1 w:v) and stirred. The sample is left for 1 hour and stirred occasionally.

To prepare the Orion Star™ A121 Portable pH Meter, which is to be used with the Orion™ ROSS™ Sure-Flow™ pH Electrode with Sure-flow junction, BNC connector, the electrode must be cleaned and calibrated. To clean, the electrode is rinsed with DI water, and then a 3-point calibration with 4.01, 7.0, and 10.01 buffer solutions is performed.

After 1 hour, the sample is stirred for 30 seconds, and then the pH is measured and recorded.

On-Site: CaCl₂ Solution pH

Using the soil-water slurry, 10 mL of 0.02 M CaCl₂ is added to soil suspension. The sample is stirred and stands for at least 15 minutes. The sample is stirred again, and the pH is measured and recorded. A constant of 0.6 is added to the CaCl₂ pH as a correction factor to compare with the water pH (Soil Survey Staff 2022).

Laboratory: Soil-Water Slurry

Soils are sent from the farm to Kling Geology Laboratory at Yale University. To measure pH on the samples received, at least 10g of each soil sample are dried in a drying oven at 60C for 48 hours, then sieved through as 10 mesh (2mm) sieve. The sieved sample is weighed and 10g are measured into a 50mL falcon tube. Then, 10mL of milliQ₂ water is added to the sample and the sample is shaken vigorously for one minute to homogenize and left to stand for 10 minutes. Then, pH is measured using a cleaned and calibrated Orion Star™ A121 Portable pH Meter with the Orion™ ROSS™ Sure-Flow™ pH Electrode with Sure-flow junction, BNC connector probe.

Laboratory: Sikora buffer pH

To measure the buffer capacity, the Sikora buffer pH methodology is employed (Sikora 2006). Using the sample on which soil-water pH was just measured, 10 mL of Sikora buffer solution is added to the soil suspension and shaken in an Eberbach shaker table for 10 minutes at 180 oscillations/minute. The pH is measured again.

Results

Spatial Variability

Soil pH was measured both on-site using two different methods, and in the laboratory using two different methods. The pH of individual sample points is given in the maps below, adapted from code developed by Jake Jordan.

Figure 7 illustrates soil pH, taken on-site using a CaCl₂ slurry, in April, just after basalt application and in August, 3 months after application in plots A and B. According to the CaCl₂ method, the average soil pH in plot A (control) was 6.80 +/- 0.50, with a range of 6.19 to 7.24 in April. In August, the average pH was 6.90 +/- 0.30, with range 6.39 to 7.28. In plot B (25 t/ha), soil pH average was 6.40 +/- 0.40 with range 5.86 to 6.97 in April and average 6.90 +/- 0.3 6.46 to 7.35 in August.

Figure 8 demonstrates the variability of pH in plot A, B, and D in March and in October, as measured on soil samples in the laboratory. The top two plots show pH taken from a soil water slurry, while the bottom two graphs show Sikora buffer pH, both in a laboratory setting.

In March, the mean Sikora buffer pH in the control plot was 6.93 +/- 0.04, with a range from 6.6 to 7.18. The Sikora buffer pH of the low basalt application (7 t/ha) plot was 6.84 +/- 0.33, and the Sikora buffer pH of the high basalt application plot (25 t/ha) was 7.05 +/- 0.20.

In October, the mean Sikora buffer pH in the control plot was 6.96 +/- 0.07, with a range from 6.34 to 7.28. The Sikora buffer pH of the of low basalt application (7 t/ha) plot was 6.87 +/- 0.50 with a range from 5.49 to 7.52. The Sikora buffer pH of the high basalt application plot (25 t/ha) was 7.14 +/- 0.2 with a range from 6.76 to 7.37.

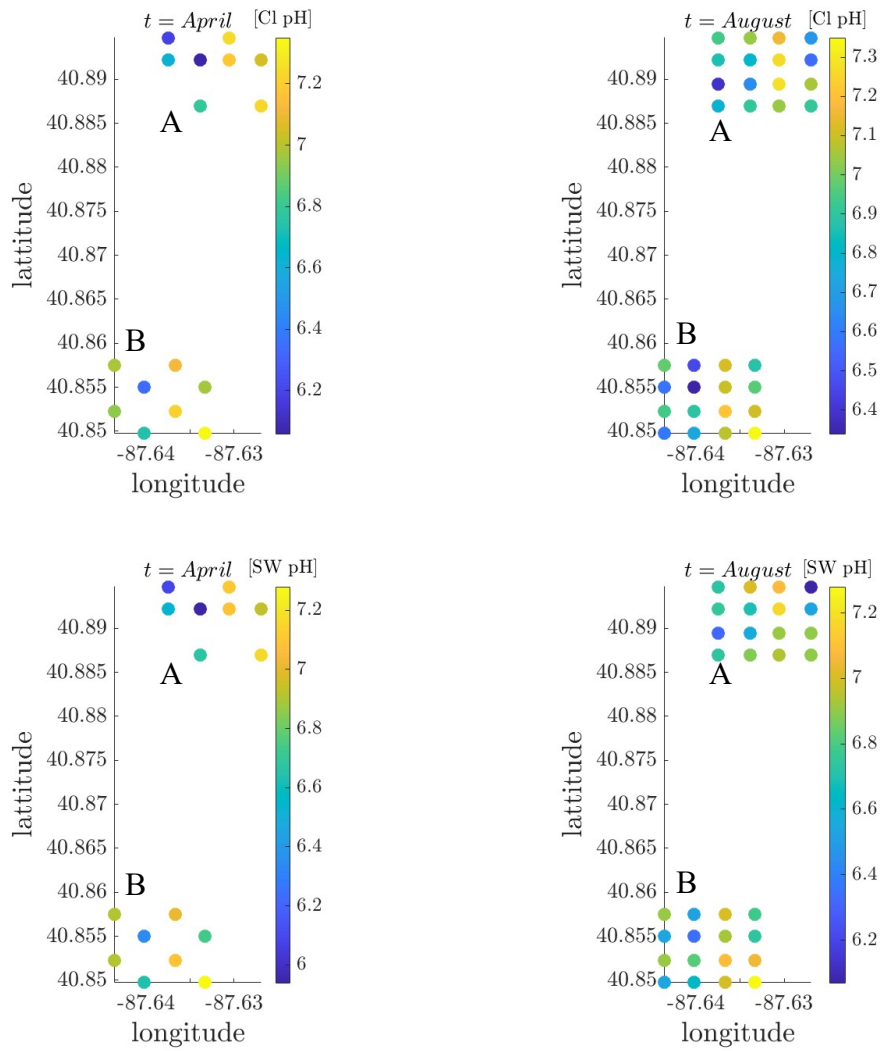


Figure 7: Soil pH of samples within plot A (control) and plot B (25 t/ha) in April 2022 and August 2022. The top plots give pH as measured on the farm using a soil water slurry and the bottom plots give pH as measured using a CaCl₂ slurry.

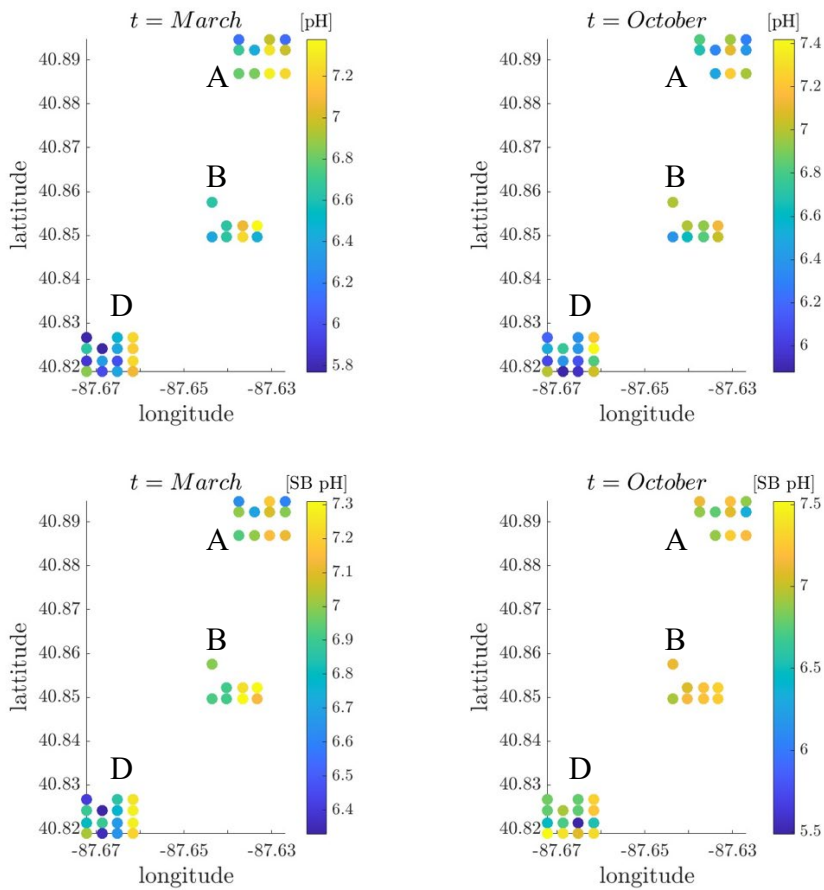


Figure 8: Soil pH of samples within plot A (control), plot B (25 t/ha), and plot D (25 t/ha) in March 2022 and October 2022. The top plots give pH as measured in the laboratory using a soil water slurry and the bottom plots give pH as measured using the Sikora Buffer method.

Temporal Variability

Figure 9 shows the change in pH over time, as measured in a CaCl₂ slurry on the farm in plots A-G between April to August.

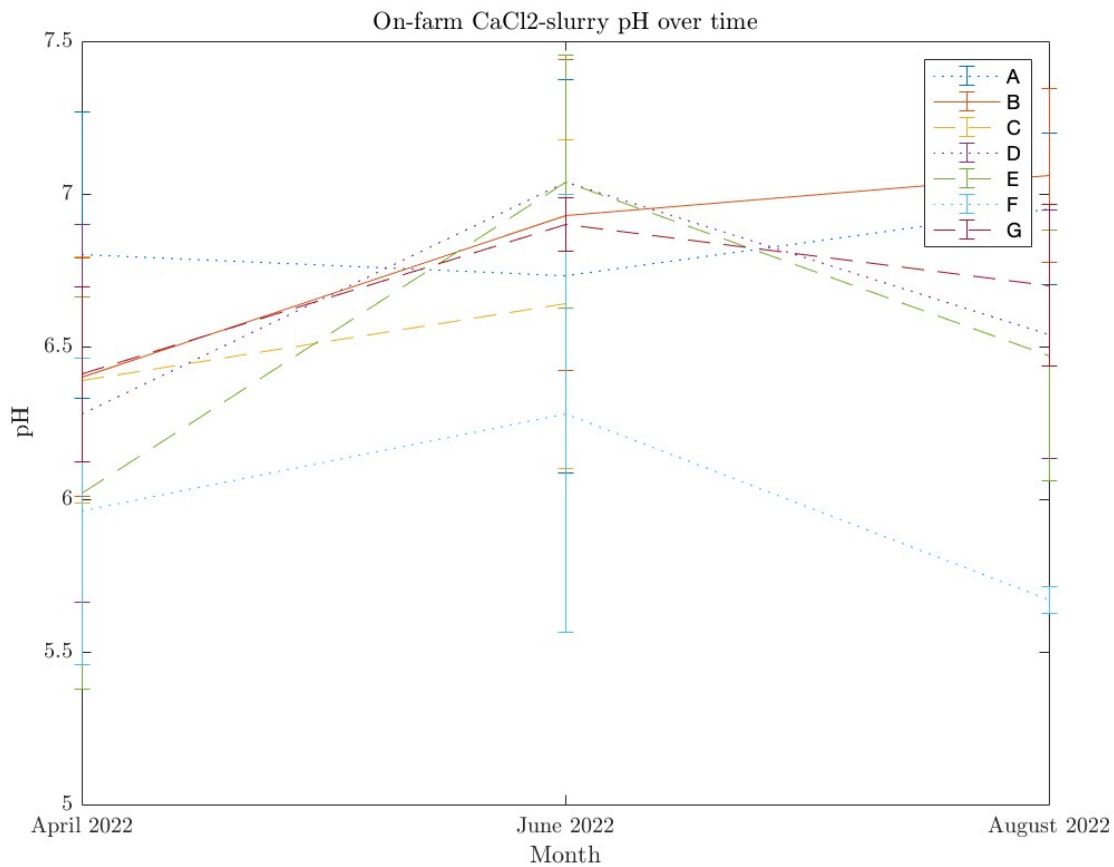


Figure 9: pH over time as measured on-site using a CaCl₂ slurry. Dotted lines are control plots, dashed lines are 7 t/ha basalt plots, solid line is a 25 t/ha basalt plot.

Statistical Analysis

Comparing plots A, B, C, and D in March, June, August, and October, there was no statistically significant difference in soil water pH or Sikora buffer pH, as measured in the laboratory, between plots (see table 4) in any month. However, if only plot A (control) and plot B (25 t/ha) are compared, the Sikora buffer pH in October was statistically significantly different, with a p-value of 0.02. However, the change of Sikora buffer pH in plot B vs plot A was not significant ($p =$). In plot B (25 t/ha), Δ pH using Sikora Buffer method was 0.07 +/- 0.12 between March and October, while Δ pH using Sikora Buffer method in plot A (control) was 0.06 +/- 0.07.

P-Values from One-Way Anova Comparing Buffer pH Between Plots

	SW pH A-B	SB pH A-B	SW pH A-B-C-D	SB pH A-B-C-D
March	0.79471	0.40631	0.16289	0.39184
June	0.32854	0.90925	0.18435	0.93043
October	0.98432	0.55682	0.49411	0.65835
August	0.11559	0.024421	0.051049	0.15439

Table 4: Test for statistical significance in Sikora buffer pH between plots using one-way Anova

Comparing plots A, B, C, and D in March, June, August, and October, there is statistically significant difference in soil water pH, measured on the farm in March and in August, but not statistically significant different in June or October (see table 5). Using the CaCl₂ method, only March showed a significant difference in pH between plots, and this was before basalt application. Looking at only plots A and B, no statistically significant difference is observed in either pH method in any month.

P-Values from One-Way Anova Comparing On farm pH Between Plots A-B-C-D

	SW pH	Cl pH
March	0.033524	0.11161
June	0.44427	0.2888
July	0.34277	0.23801
August	4.2779e-06	8.1577e-07

Table 5: Test for statistical significance in on-farm pH between plots using one-way Anova

Discussion

A spatial gradient can generally be seen across each plot for all pH measurements, sample plots, and sample dates indicating a correlation between pH and natural soil variation (i.e. due to drainage, soil type, temperature, etc). The standard deviations within plots are relatively low (< 0.5), in comparison to crops' pH tolerance. For corn, crop yields are not significantly impacted when pH is between 6-7.4 (Fernández and Hoefl 2009). Still, in some cases, variation of more than one unit of pH is seen even between sample locations less than 20m apart.

Overtime, a general trend of increasing pH, as measured on the farm in a CaCl₂ slurry, with increasing basalt application is observed, as in figure 9. However, based on an ANOVA test on change in CaCl₂ pH and in Sikora Buffer pH, there is no statically significant difference.

Sikora buffer pH is useful in assessing the effect of enhanced rock weathering because it provides an indication of the buffering capacity of the soil, or the amount of residual acidity in the soil that is available to be neutralized. A lower buffer pH means there is more residual acidity in the soil that would react with weathering basalt. Sandier soils tend have a lower buffering capacity which means that they acidify faster but would recover faster with the application of less basalt or lime, compared to soils with more clay.

The pH in all the plots began close to neutral, so it is unsurprising that pH was not changed significantly as a result of basalt application. Around pH of 7.0, silicate rocks weather more slowly. For example, figure 10 shows Si release rates from weathering at varying pH values. The basalt that was applied is predominantly plagioclase meaning it weathers slowly between pH 5.5 – 7.5 (Gudbrandsson et al. 2011).

Given that there was not a consistent trend in difference in pH or change in pH over time between control and test plots, it is reasonable to assume that pH differences that were observed should be attributed to other variations within the site.

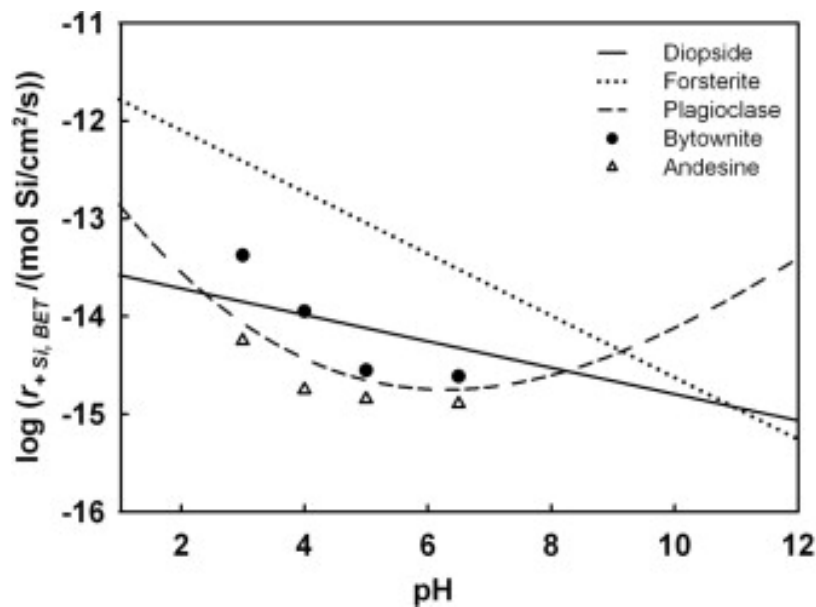


Figure 10: release rates of selected minerals at 25 °C as a function of pH (Gudbrandsson et al. 2011).

In theory, cation loss due to weathering should be predicted by change in pH over time, according to the governing equation: $\text{CaSiO}_4 + \text{H}^+ \rightarrow \text{Ca}^{2+} + \text{HSiO}_4$. Here, CaSiO_4 is used as a placeholder for a more complex basalt compound. $\text{pH} = -\log [\text{H}^+]$, so the change in $[\text{H}^+]$ can be calculated based on the pH, and the equivalent number of moles of Ca^{2+} would be expected to be found in the aqueous solution as a result of weathering, according to stoichiometry. Change in cation concentration (i.e. cation dissolution), measured in mol/ha, was found to not be significantly different between control and test plots, as predicted by the lack of change in pH.

A primary concern from farmers about applying heavy applications of basalt, in comparison to the typical lime application rate (around 2-5 t/ha every four years), is the potential to increase pH significantly above neutral. This was not observed, even with the high application rate of 25 t/ha.

Applying basalt for ERW on fields that already have a pH that is close to neutral will likely not have as significant impacts on crop yields, while it is predicted to increase yields in acidic fields. While this is good for farmers, in soils that have been acidified by excess nitrogen fertilization (as is common in conventional midwestern cropping systems), cations in the basalt are likely to react with nitric acid in the soil, in addition to carbonic acid, therefore reducing CDR potential (Andrews and Taylor 2019).

Section 2: Yields

Methods

Site #1

To measure yields, two subplots of 0.3 hectares each (subplot size was determined based on machinery dimensions), were designated in each test plot. The weight of beans harvested from each plot was then recorded using a weigh wagon.

Sites #2 and #3

Yields were not measured in sites #2 and #3 to date because basalt has not yet been applied.

Site #4

Site #4 is a pasture, so yields were not measured.

Site #5

To measure yields, hay bales from a subset of each plot, allowing for buffer zones between plots, were weighed by hand on a scale as they were removed from the field. Oat seed was weighed in a weigh wagon.

Site #6

In year one, corn was grown on this plot and yield were measured similarly to site 1: delineating subplots to measure grain with a weigh wagon. In year two, buckwheat was grown, but yields were not measured.

Results

In site #1, the soy yield in the low application rate test plot (7 t/ha) saw a 1.8% increase in yield while the high application rate (25 t/ha) saw a 0.28% increase, both compared to a control plot. Due to the small sample size, and this small difference, the correlation between basalt treatment and soy yield cannot be determined with confidence.

While the focus of this report is on site #1, yield data from other sites in this study are included to better represent the varying effects basalt has on crop yields, depending, in part, on crop type.

Soy Yield with Varying Basalt Application Rates

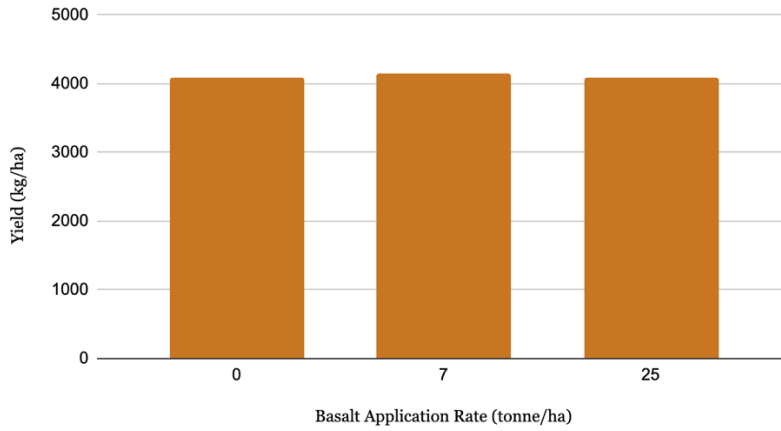


Figure 11: Effect of basalt in Site #1 on soybean yield in 2022 growing season.

Corn Yield with Varying Basalt Application Rates

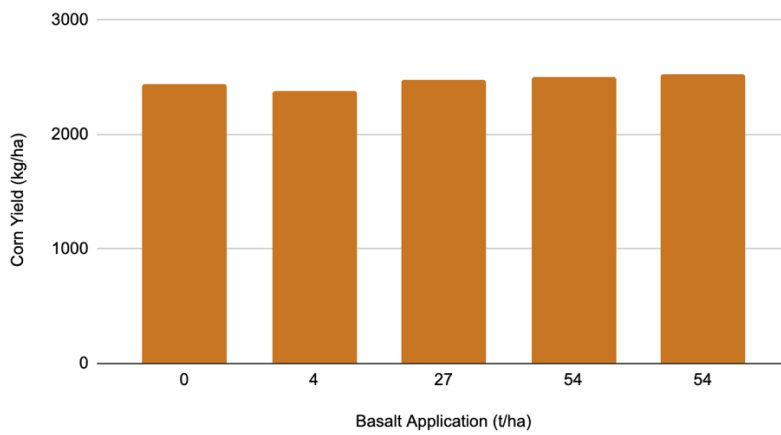


Figure 12: Effect of basalt on corn yield in Site #6 in 2021 growing season.

Oat Yield Increase

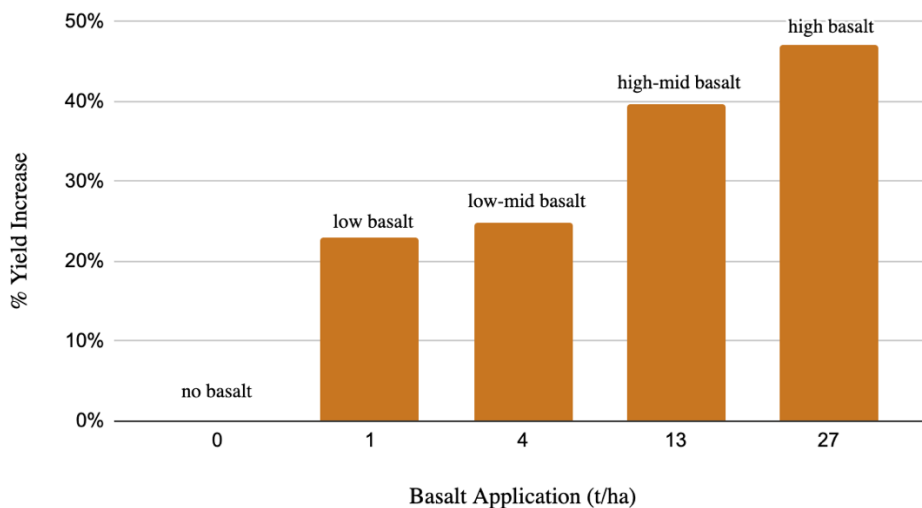


Figure 13: Effect of basalt on oat yield in Site #5 in 2021 growing season.

Discussion

Site #1

A primary reason for increased yields due to basalt application is pH neutralization. This was not needed in site #1 as the baseline pH was close to zero, so it is expected that yields would not have a significant impact. There is no published data to date on the effect of ERW on soy yields based on field trials. In an incubation test though, addition of crushed basalt was shown to increase available phosphorus, potassium, calcium, and magnesium levels by twenty, ten, fifteen, and thirteen times respectively, and, soy was observed to accumulate five times more macro and micronutrients (Conceição et al. 2022).

Site #5 and #6

While smaller scale, sites #5 and #6 provides valuable insight into the effect of basalt on hay and corn yields. On 4.9 hectares in site 5, hay field was established with oats, alfalfa, timothy in 2021. On 3.2 hectares in site #6, conventional corn was grown in 2021.

The significant jump in oat yields is likely due to a limiting micronutrient, such as molybdenum, but further research is needed to constrain the casual effect of basalt on oat yields.

In the future it will be important to utilize moisture correction when comparing hay yields. It became clear that there was significant variation within the field—some areas included clover that had self-seeded, some areas were dominated by timothy, and other areas were dominated by alfalfa, despite uniform planting. Alfalfa, timothy, and clover each retain different levels of moisture, therefore obscuring the yield data. This challenge also introduced a question as to whether basalt addition impacted the prevalence of alfalfa versus timothy vs clover. A future study could investigate if certain hay crops are better suited to basalt.

Because of the lack of moisture correction and small-scale of this study, this data should be used only as an initial indication of positive correlation between oat and hay yields and basalt. One control plot had anomalously high yields, and that plot had notably higher levels of clover compared to all other plots, and clover retained noticeably more moisture than timothy or alfalfa, so it was excluded from the graph above. That plot was previously pasture while the other plots had been in corn/soy rotation for longer, so the baseline conditions were likely not comparable.

In 2022, alfalfa and timothy grew again as they are perennials. During the first harvest of the 2022 season in June, a general trend was observed of increasing yields with increasing basalt application. Yields during the second harvest in July demonstrated less variation across plots.

The effect of basalt on corn yields (~3% crop yield increase) is similar, or slightly lower, than the predicted crop yield increase as a result of liming (Inagaki et al. 2016). A study conducted in Denmark on a corn field treated with glacial rock flour, a different silicate-based mineral, demonstrated a statistically significant ($p = 0.018$), though small (roughly 0.05%) increase in corn yield (Gunnarsen 2023). Similar to soy, in an incubation study, corn was observed to accumulate five times more macro and micronutrients (Conceição et al. 2022), which suggests that at scale crop yields would increase with basalt application, and the need for synthetic fertilizers would be reduced.

Section 3: TiCat

Methods

Extracting Exchangeable Cations

Before sample analysis, the fraction of exchangeable cations in the sample are extracted. Samples are dried by measuring approximately 500mg of each soil sample into a labeled crucible and placing crucibles into the oven set to 60°C overnight. Then, 100mg of dried sample is measured into labeled 15 mL centrifuge tubes. The exact mass of each sample is recorded. Then, 12mL of 1 M Ammonium Acetate buffered to a pH of 8.2 is added to each 15 mL centrifuge tube. The tubes are shaken vigorously for one minute each and placed into racks for a sonic bath. The sonicator runs for 10 minutes. After sonication, the tubes are removed, dried, and placed into a centrifuge to be run for 5 minutes at 3600 RPM. At this point, the soil is stuck firmly to the bottom of the tube and the ammonium acetate solution is poured into clean labeled centrifuge tubes. Two mL of milliq water is then added to each centrifuge tube containing soil and mixed vigorously for one minute. The tube is then placed into the centrifuge and runs for 5 minutes at 3600 RPM again. Then, the solution is poured out into the same tubes which contained the ammonium acetate solution.

For each sample, the weight of a crucible is recorded and the crucible is labeled. The soil sample is removed from the tube and placed into the crucible. The soil sample is then dried again in an oven at 65°C overnight. The samples are then removed from the oven and the mass of each crucible plus dried sample is recorded.

Samples are then ashed by placing crucibles in the oven overnight at 600°C. The ashed sample is then weighed again in its crucible. The difference in mass of the sample before and after ashing provides the mass of organics and volatiles in the sample.

The ashed sample is weighed again and put into a Teflon beaker.

Total Acid Digest

After ashing, the samples are digested. To each sample, 5mL distilled HNO₃ and 5mL distilled HCL is added. The samples are left open in a closed fume hood for one hour. Then, 1 mL of HF is added to each sample, the samples are capped and placed on a hot plate at 100°C overnight or up to 24 hours. The samples are opened slowly and placed back on the hot plate, increasing the temperature to 90°C such that the liquid fully evaporates. The samples are capped and removed from the hot plate to be placed in a fume hood. Then, 4 mL of 6N HCl is added to each sample. The samples are capped again and placed on a hot plate at 75°C overnight or up to 24 hours. The samples are then removed from the hot plate and left to cool for 20-30 minutes. The digested samples are transferred to labeled 15 mL Nalgene bottles.

Isotope Spike Cocktail

In clean silver crucibles, 0.28 mg of SiO₂ powder enriched with ²⁹Si isotope (99.96%, Isoflex USA) is mixed with NaOH pellets (analytical grade, Merck, ca. 220-240 mg). Alkaline fusion is carried out in a muffle furnace at 730°C for 10 min. The crucibles are taken out and allowed to cool for 1 min before being placed into 30 ml Teflon Savillex beakers containing 20 ml

deionized water. The beakers are placed for 24 h in a hot plate at 70°C and then ultrasonicated three times for 15 minutes. Then, the crucible contents are dissolved into 414.3517 ml of seawater (pH 7.67). pH is immediately adjusted by the addition of HCl 1 N to reach a pH of 7 and measured using a Thermo Scientific™ Orion™ 8103BN ROSS™ Combination pH electrode, calibrated using NIST-traceable 4.01, 7 and 10.01 pH buffers.

Elemental Analysis

To prepare samples for ICP-MS analysis, 40 microliters of digested samples are pipetted to labeled 4 or 5mL Teflon beakers. Teflon beakers are then placed on a hot plate, uncapped, at 85-90°C for 1-2 hours, to evaporate liquid. Samples are removed from the hot plate once the liquid is evaporated, and 3.99 mL of 5% HNO₃ without indium is pipetted into each sample. Then, 20 microliters of isotope spike cocktail (see above) is pipetted into each sample. Lids are closed tightly, and samples are heated on a hot plate at 75°C for 1-2 hours. Then, samples are transferred to labeled 4 mL plastic vials. Samples are run on a Thermo Scientific™ iCAP™ RQ ICP-MS.

TiCAT Framework: Solid sample mass balance approach

To determine carbon dioxide removal, a method referred to as the TiCat framework is employed (Reershemius et al 2023). The TiCat framework compares titanium (Ti) and cation (Cat) concentrations in the soil from a baseline sample, taken prior to application, to concentrations in the soil from a post-application sample, after weathering has occurred. Ti is considered immobile, meaning that after a Ti-rich supplement (e.g. basalt) is applied, the Ti is expected to remain in the soil, in relatively the same location. Cations, on the other hand, are expected to dissolve as a result of weathering and be carried off the field in water. It is assumed that weathering due to basalt application occurs at a much faster rate than natural background weathering of cations in the soil.

Similar approaches have been used for weathering in natural systems (Brimhall 1987; Chadwick 1990). It is predicted that basalt application will increase [Ti] in the post-application sample as compared to the baseline sample. The increase in [Ti] can be used to determine how much basalt was added to the soil in the specific location where the sample was collected. This is calculated using [Ti] in the baseline soil, [Ti] in pure basalt, and employing a linear mixing model to predict how much Ti would appear in samples, given a baseline soil/pure basalt ratio (see Figure 14). Based on the expected basalt concentration and the mixing model, the expected cation concentration, neglecting weathering, can be calculated. The difference between the measured cation concentration and the expected cation concentration neglecting weathering, is then used to determine the extent of weathering. A stoichiometric ratio can then be used to determine extent of carbon dioxide removal, based on cation loss.

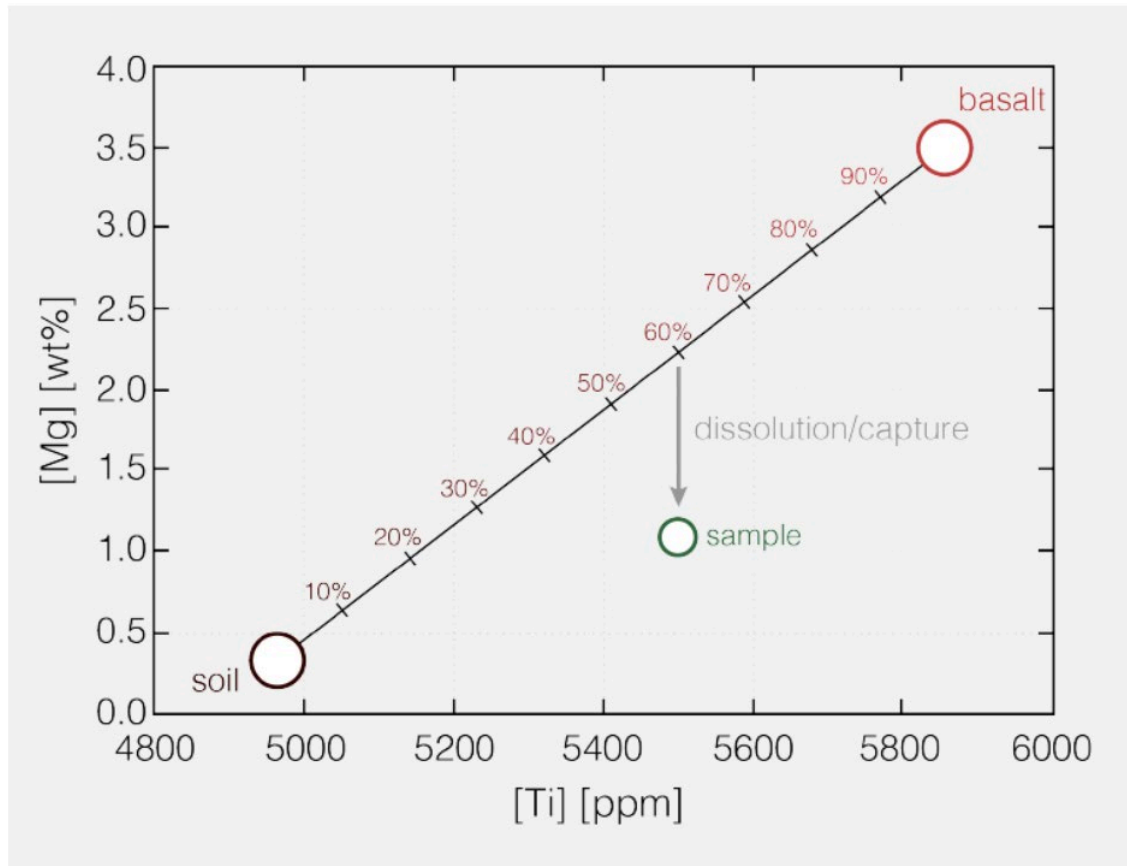


Figure 14: conceptual framework for calculating cation dissolution, exemplified by Mg. Dissolution is illustrated by the gray arrow (difference between [Mg] predicted by the linear regression of [Ti] vs [Mg] and measured [Mg] in the post-application sample)

This framework assumes that change in Ti and cations is due exclusively to basalt application and weathering, and that no third component (e.g. other soil types, compost, etc) is introduced to the soil between baseline sample and the post-application sample dates.

Comparison of measured data to expected values

The expected amount of basalt in a given soil sample, assuming “perfect application”, can be calculated and compared to the amount of basalt predicted by measured values to assess the extent to which measured values fit the assumptions of the TiCat framework. Here, “perfect application” means that the basalt feedstock was spread in a uniform sheet across the amended field, there is constant density of the soil (ρ_s) and basalt (ρ_b), and the basalt is completely and uniformly mixed with the top 10 cm (sample depth) of soil through tilling.

The thickness of the basalt layer, h_b , can be calculated using the application rate of basalt and the density. Assuming an application rate, A [kg/m²], the thickness of the basalt layer is given by

$$h_b = A \cdot \rho_b (1)$$

Accordingly, in this model, a sample taken to the depth of tilling is assumed to include the entirety of the basalt application. Samples analyzed in this study were taken at the same depth as tilling (10cm). The portion of the cored sample that is soil without basalt (h_s), given sampling depth (h_d) and thickness of basalt layer (h_b) is expressed as

$$h_s = h_d - h_b$$

The terms h_x have units of length. The volume can be calculated as the cross-sectional area of the sample soil core (A_{core}) is assumed constant.

$$h_s \times A_{core} = V_s \text{ and } h_b \times A_{core} = V_b \quad (2)$$

Using ρ_s and ρ_b the mass fraction of soil (x_s) and basalt (x_b) may be calculated

$$x_s = \rho_s * V_s / (\rho_s * V_s + \rho_b * V_b) \text{ and } x_b = \rho_b * V_b / (\rho_s * V_s + \rho_b * V_b) \quad (3)$$

x_s and x_b can be used to predict $[Ti]$ and $[Cat]$ of a post-application sample, based on elemental composition of the baseline soil and basalt.

$$[Ti]_i^* = x_s * [Ti]_i^{t,0} + x_b * [Ti]_i^f \quad (4)$$

$[Ti]_i^*$ = expected value for Ti concentration of sample

$[Ti]_i^{t,0}$ = measured value of Ti concentration in baseline soil sample (prior to application)

$[Ti]_i^f$ = measured value of Ti concentration in basalt feedstock

The difference between measured and expected $[Ti]$ in a post-application soil sample taken after weathering has occurred, is given by:

$$\Delta^* [Ti]_i = \left(\frac{[Ti]_i^{t,f} - [Ti]_i^{t,0}}{[Ti]_i^* - [Ti]_i^{t,0}} \right) - 1. \quad (5)$$

Equation (5) is positive if the measured $[Ti]_f$ exceeds the expected value, negative if it is lower than expected, and zero if it is identical. If $\Delta^* [Ti]_i$ is less than -1 than $[Ti]_f$ is less than $[Ti]_i$ and the assumptions of mass balance fail. Since a Ti-rich supplement (basalt) is added to the field between the $[Ti]_i$ measurement and the $[Ti]_f$ measurement and it is assumed that nothing else changed the soil in that timeframe, it is impossible that $[Ti]_f < [Ti]_i$ according to our assumptions. Therefore, either an accounted for process occurred between sampling that led to a decrease in $[Ti]$, or more likely, insufficient sampling led to misrepresentative data.

The operations in Equations (4) and (5) can be applied to base cations as well. However, titanium is considered an immobile element while cations are not, so Equation (5) represents a value that is assumed fixed through time. If this is not the case (i.e., the value of $\Delta^* [Ti] < -1$ suggesting that Ti increased after basalt application and then decreased again, or that the data simply does not represent the actual change in Ti), then the mass balance calculation cannot be computed. Base cation values are expected to decrease with time as weathering causes base cations to be

exported from the system. This calculation would give insight into the expected cation concentration after application, prior to weathering.

Results

Ti and Cation Concentrations Across Individual Sample Points

The following graphs illustrate [Ti] and [Cat] in plots A (control), B (25 t/ha), and D (7 t/ha) before basalt application and six months after basalt application. In addition, the measured change in concentration ($\Delta[X]$), and the measured change in concentration as a fraction of predicted change ($\Delta^*[X]$) is shown.

Only a subset of data points are shown because only a subset of soil samples have been analyzed using the methods described above to date. One plot from control, low application rate, and high application rate, was prioritized before analyzing samples from additional plots.

In figures 17, 19, and 21, post-application sample cation concentrations are shown in reference to a range of expected concentrations, given by the shaded red triangle. The shaded region is determined based on a two-component mixing model between baseline soil composition and basalt composition. Ti is expected to be immobile so the Ti concentration is expected to be constant over time. This is illustrated by zero $\Delta^*[Ti]$ (gray dots) in the control plots, shown in Figure 15. It is assumed that Ti should increase from pre-application baseline soil to post-application sample and 100% of Ti addition is due to basalt application. So, the amount of basalt in each soil sample is calculated based on $\Delta[Ti]$ between pre-application and post-application. In each graph in figures 17, 19, and 21, the horizontal line represents baseline soil cation concentration, and the diagonal line represents expected cation concentration, given a Ti concentration, before weathering (i.e. shortly after basalt application). Over time, cation concentration is expected to decrease due to weathering, while [Ti] remains constant. Therefore, six months after application (i.e. October samples), the data points are expected to fall within the shaded red triangle.

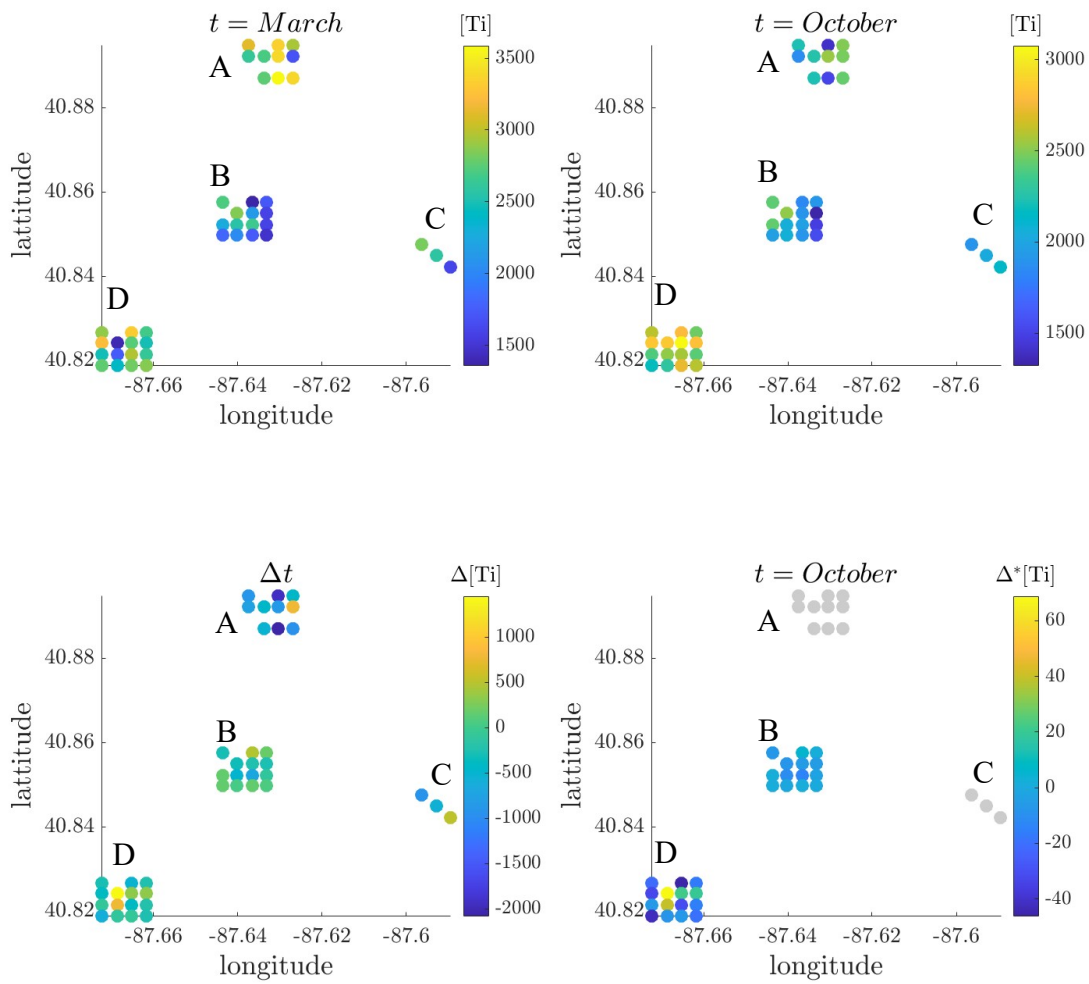


Figure 15: Titanium concentration in March and in October (top graphs). $\Delta[\text{Ti}]$ and $\Delta^*[\text{Ti}]$ between March and October (bottom graphs). Dots in gray represent null values because no change in concentration is expected, making the denominator for $\Delta^*[\text{Ti}] = 0$.

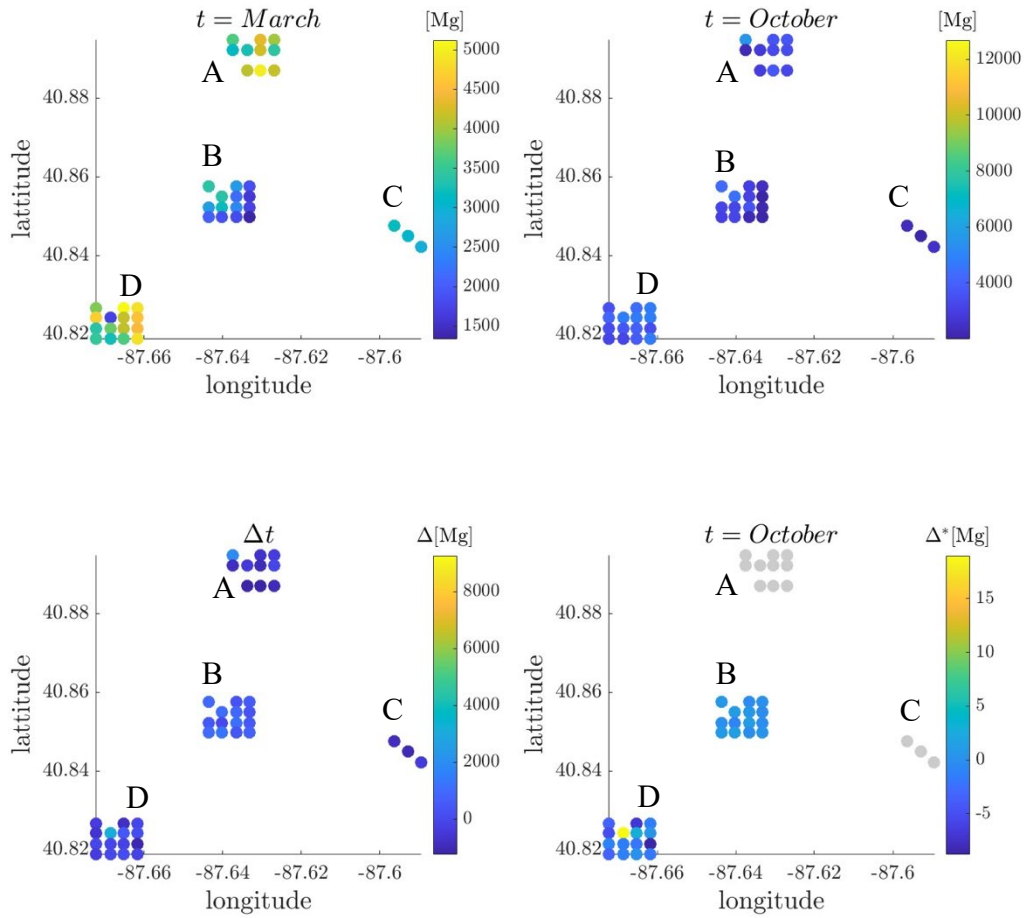


Figure 16: Magnesium concentration in March and October (top plots). $\Delta[\text{Mg}]$ and $\Delta^*[\text{Mg}]$ between March and October (bottom graphs). Dots in gray represent null values because no change in concentration is expected, making the denominator for $\Delta^*[\text{Mg}] = 0$.

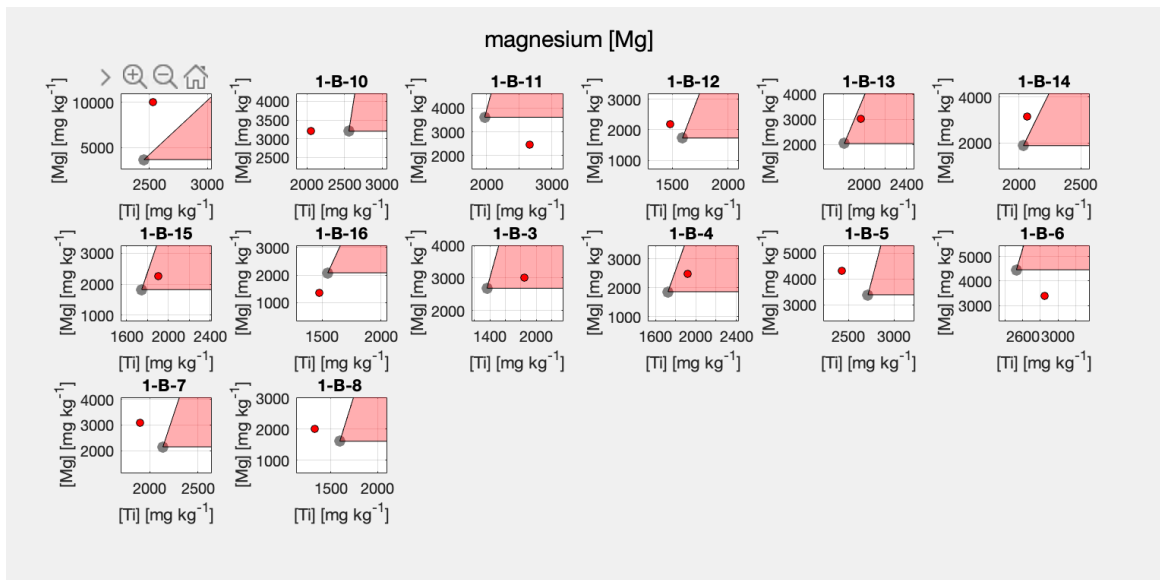


Figure 17: Visualization of [Mg] of a given sample point (red dot) in reference to expected concentration range (shaded red zone) within plot B (25 t/ha).

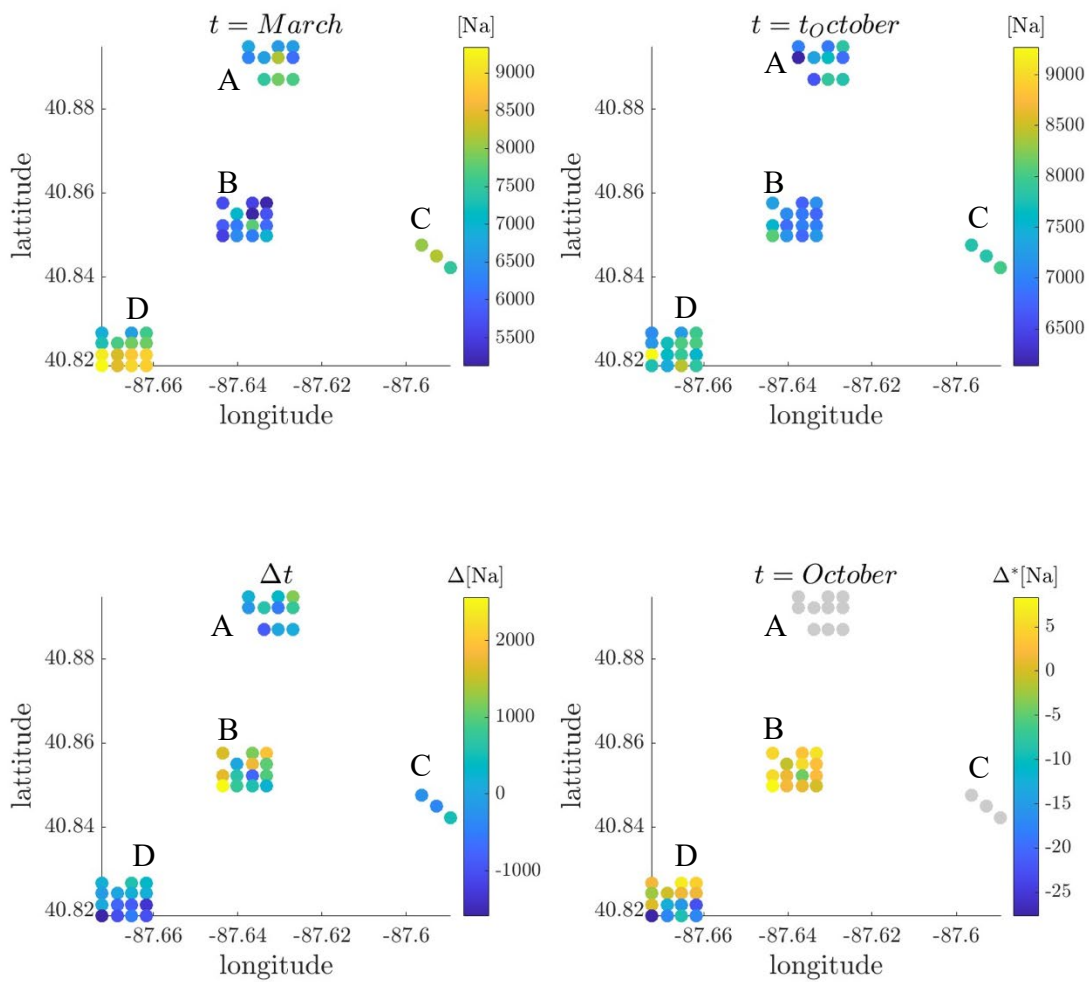


Figure 18: Sodium concentration in March and October (top plots). $\Delta[Na]$ and $\Delta^*[Na]$ between March and October (bottom graphs). Dots in gray represent null values because no change in concentration is expected, making the denominator for $\Delta^*[Na] = 0$ (bottom plots).

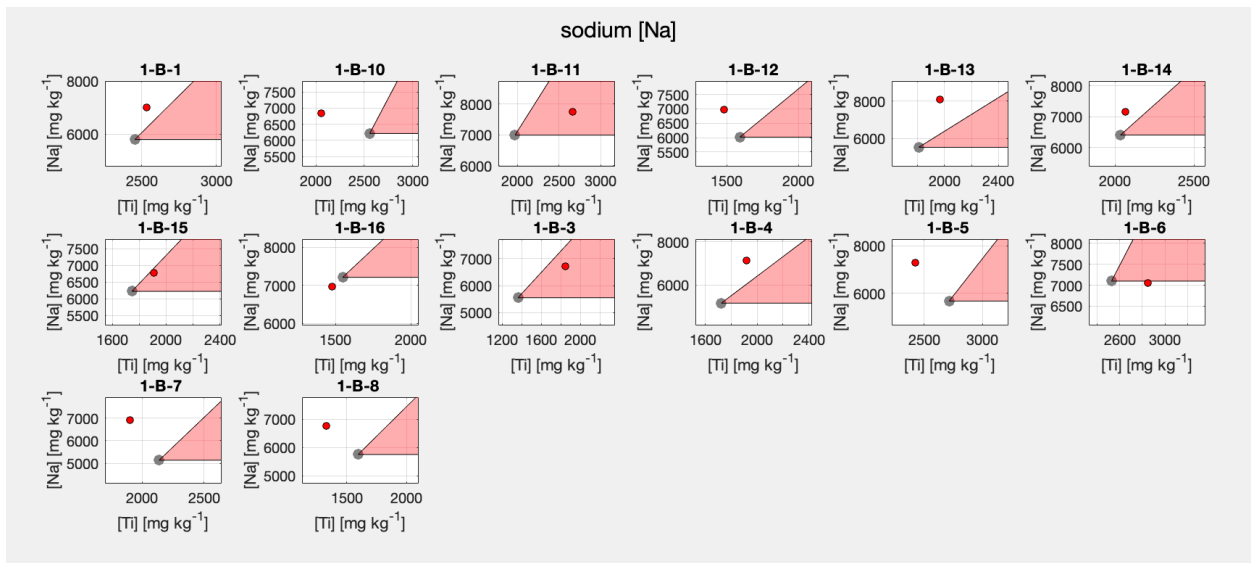


Figure 19: Visualization of [Na] of a given sample point (red dot) in reference to expected concentration range (shaded red zone) within plot B (25 t/ha).

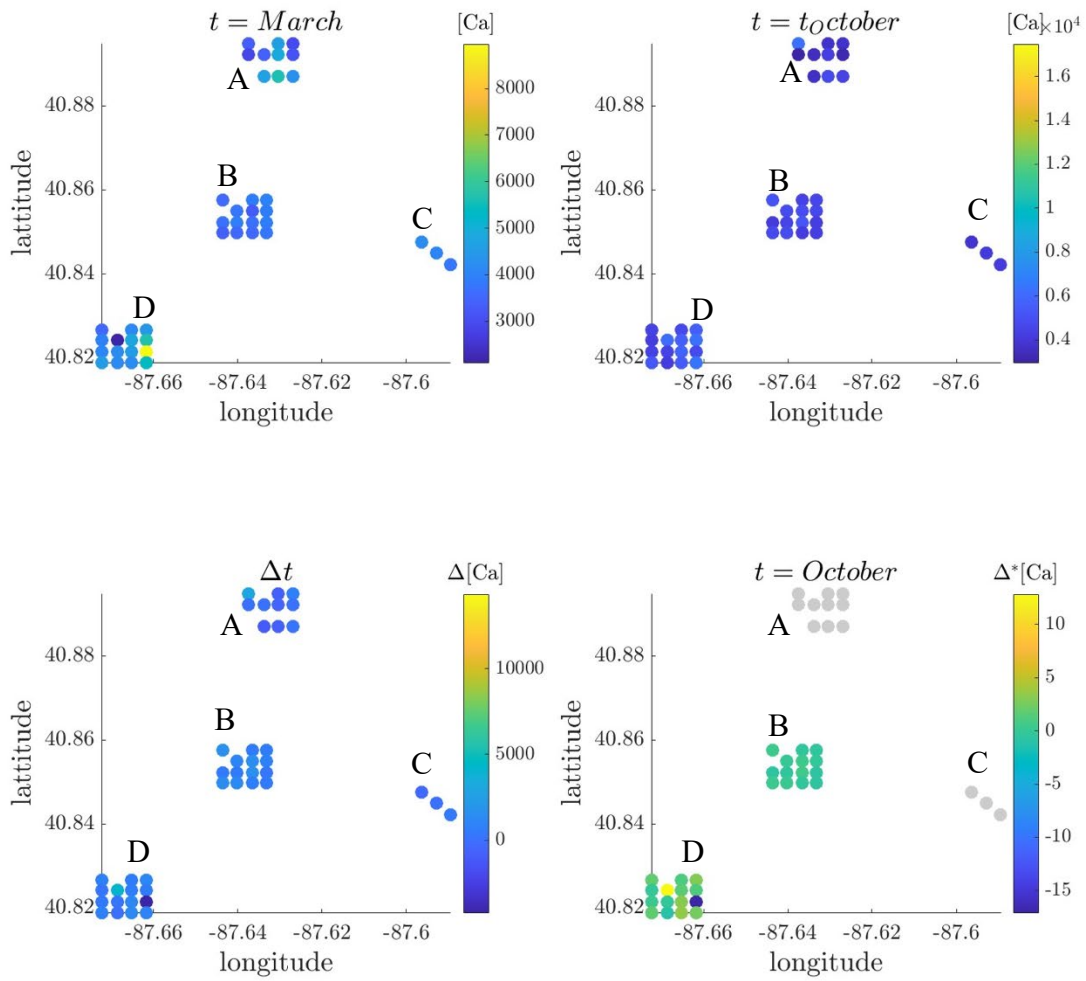


Figure 20: Ca concentration in March and October (top plots). $\Delta[Ca]$ and $\Delta^*[Ca]$ between March and October (bottom graphs). Dots in gray represent null values because no change in concentration is expected, making the denominator for $\Delta^*[Ca] = 0$ (bottom plots).

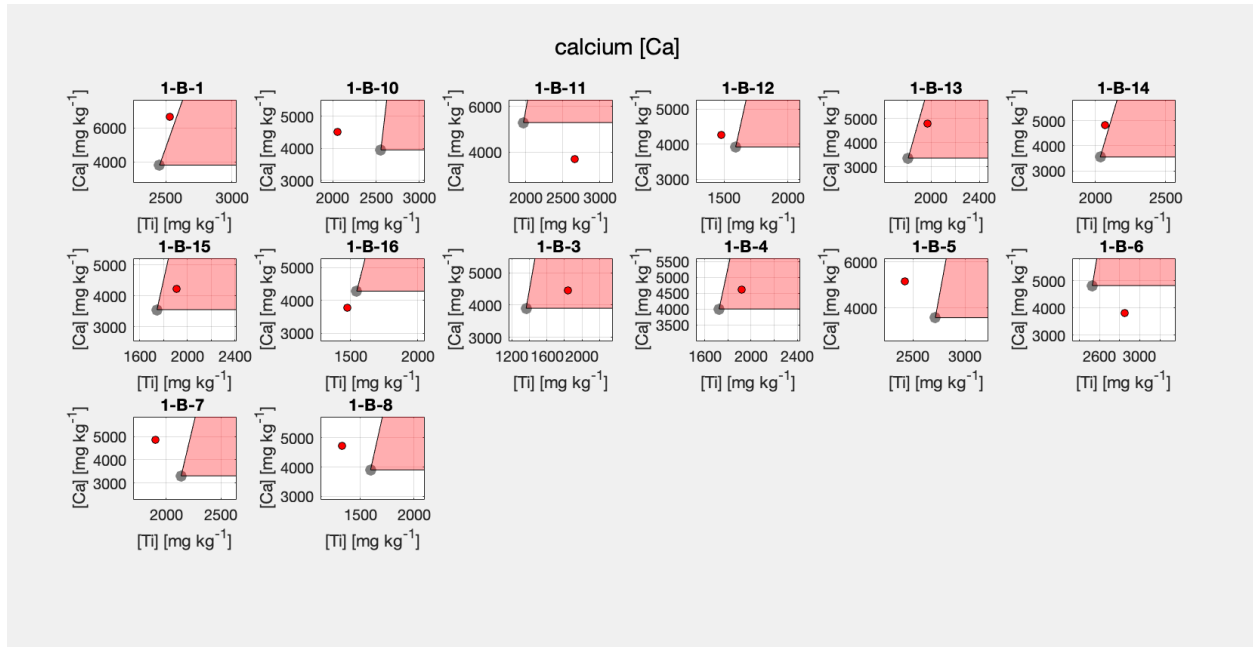


Figure 21: Visualization of [Ca] of a given sample point (red dot) in reference to expected concentration range (shaded red zone).

Cation Dissolution and Cation Loss

The percent cation dissolution (F_d^+) was calculated by finding the final cation mass fraction (in this case, 6 months after basalt application), over the sum of the final cation mass fraction and the pure basalt cation mass fraction.

The mass fraction are calculated using the system of equations given in (6). C^D is the total measured concentration of the detrital element (Ti) and C^+ is the measured total concentration of the cation (Mg, Ca, or Na), in the final soil sample (taken in October). The measured concentrations of Ti and cations in the baseline soil and the pure basalt are given by c_s^D , c_b^D , c_s^+ , c_b^D respectively. The concentration of the Ti and cations after complete dissolution (if 100% of the basalt had been weathered) is given by c_d^D and c_d^+ . These are determined by two assumptions: (1) Ti is immobile so there would be zero Ti loss and the only source of Ti gain is from the basalt, so $c_d^D = c_b^D$, and (2) background soil weathering is negligible so when all of the basalt has weathered, the cation concentration returns to the baseline soil concentration and $c_d^+ = c_s^+$. This is shown in figure 22.

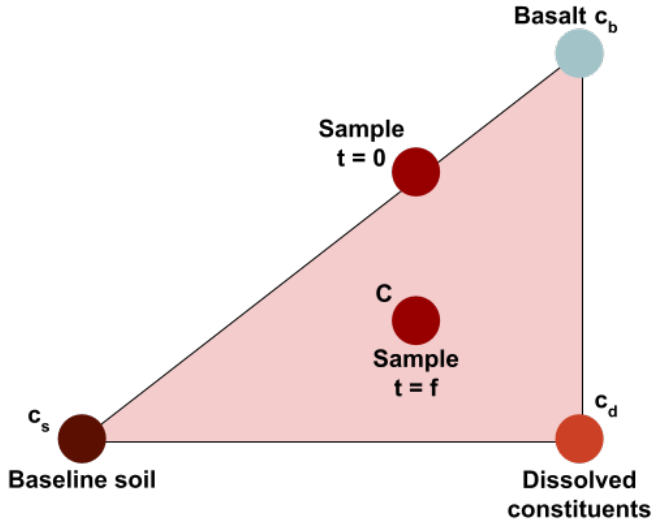


Figure 22: Visualization of mixing triangle created from baseline soil with basalt addition.

The mass fraction contributed by soil (subscript s), basalt (subscript b), or dissolution (subscript d) is given by x_i , and can then be calculated by solving the system of three equations for those three unknowns.

The dissolution factor is then calculated using equation (7). Assuming all weathering is a result of ERW (background weathering is negligible), F_d^+ give the percent of the given cation in the basalt that weathered between $t = 0$ and $t = f$.

$$\begin{aligned}
 C^D &= x_s^+ c_s^D + x_b^+ c_b^D + x_d^+ c_d^D, \\
 C^+ &= x_s^+ c_s^+ + x_b^+ c_b^+ + x_d^+ c_d^+, \\
 1 &= x_s^+ + x_b^+ + x_d^+.
 \end{aligned}
 \tag{6}$$

$$F_d^+ = \frac{x_d^+}{x_b^+ + x_d^+}.
 \tag{7}$$

100% dissolution is interpreted to mean that all cations from the applied basalt has been weathered. Greater than 100% dissolution is interpreted to mean that cations present in the soil, without application, have also been weathered. Less than 100% dissolution is interpreted to mean that a fraction of the basalt has been weathered.

The table below shows cation dissolution in plots B (25 t/ha) and D (7 t/ha), averaged across all data points from a given plot.

App Rate (t/ha)	Ca Dissolution (%)	Mg Dissolution (%)	Na Dissolution (%)
25	73	23	15
7	101	93	64

Table 6: cation dissolution in plots A, B, and D between March and October.

A one-way Anova test was applied to Mg dissolution, Ca dissolution, and Na dissolution between March and October, comparing plots A, B, and D. There was not a significant difference for Mg dissolution ($p = 0.25$), Ca dissolution ($p = 0.18$), or Na dissolution ($p = 0.97$).

Cation loss can be extrapolated from cation dissolution by multiplying dissolution by the amount of a given cation expected to have been added to the field during basalt application (based on basalt application rate and basalt composition). Table 7 gives cation loss in plots A and D.

App Rate (t/ha)	Ca Loss (mol/ha)	Mg Loss (mol/ha)	Na Loss (mol/ha)
25	26679	8054.2	3130.7
7	10430	9014.2	3839

Table 7: cation loss in plots A and D, 6 months after application

A one-way Anova test was applied to Mg loss, Ca loss, and Na loss between March and October, comparing plots A, B, and D. There was not a significant difference between plots in Mg loss ($p = 0.94$) or Na loss ($p = 0.97$), but there was a statistically significant difference in Ca loss ($p = 0.019$). This is shown in figure X.

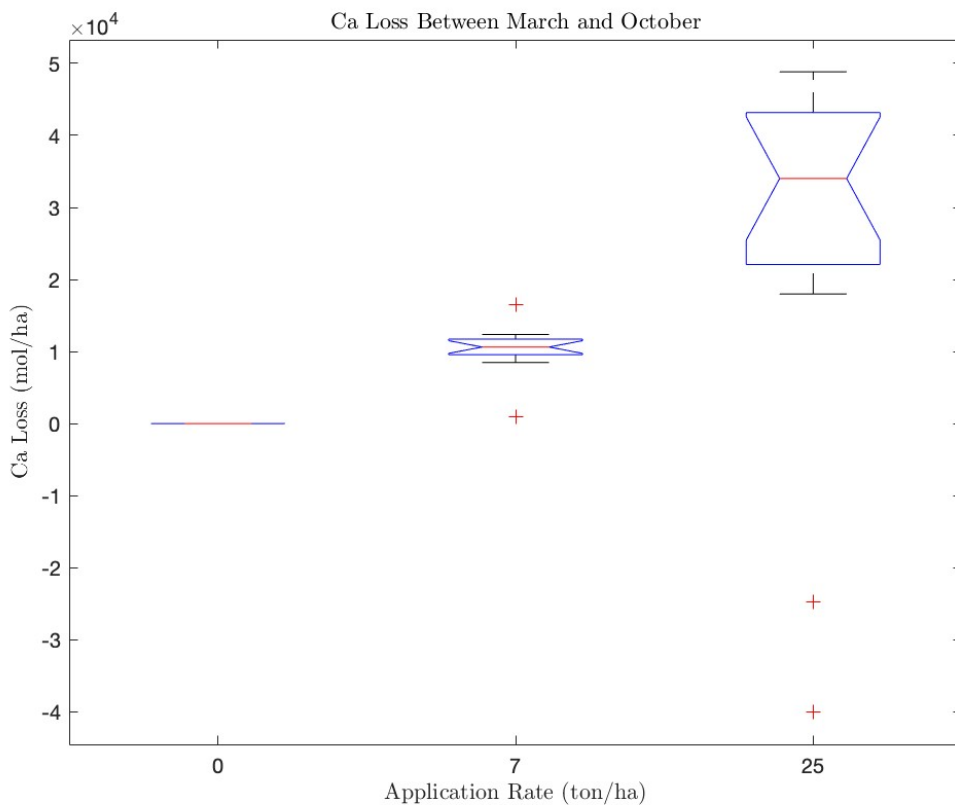


Figure 23: One-way Anova between plots A, B, and D

Carbon dioxide removal

Based on cation loss, carbon dioxide removal was estimated for plots B and D. Value (1) in Table for CDR was calculated based on the TiCAT framework, excluding data points that showed a loss in Ti between baseline soil sampling and post-application sampling. Value (2) was calculated using the same methodology as value (1) except that data points that indicated negative CDR (i.e. carbon emissions), were removed before calculating the average. A negative CDR values is outputted from this methodology when the overall concentration of cations in the post-application sample is greater than what the mixing model would predict. Value (3) was calculated using a statistical model that outputted a resampled larger data set, based on the mean and standard deviation of only measured data point that fell within expected ranges. This resampling and calculation was not done on plot D (7 t/ha) data, because it was observed that the cation loss was not significant enough, in comparison to the control plot, to make reasonable estimates of CDR.

Basalt App (t/ha)	(1) CDR (kg CO ₂ /ha)	(2) CDR (kg CO ₂ /ha)	(3) CDR (kg CO ₂ /ha)
7	1880	1880	N/A
25	3195	6527	2150

Table 8: Carbon dioxide removal based on cation dissolution

Discussion

Titanium

Ti results in Site #1 do not, overall, fit the assumptions of the TiCat framework because [Ti] decreased or remained relatively constant between March and October, as shown in the plot of $\Delta[\text{Ti}]$ in Figure 15. It is assumed that [Ti] would increase as a result of Ti-rich basalt addition to the soil.

The discrepancy between the observed and expected trend could be a result of a flooding event or other soil disturbance that led to significant movement of soil and therefore change in composition in the specific sampling location. The change in composition could mean a loss of Ti-rich soil (e.g. fine-texture soil) or gain of Ti-poor (e.g. coarse soil) soil matter, or some combination of the two.

Alternatively, the unexpected result could be indication of natural soil variation across the field. The results across the 70 x 70m plot were geospatially variable as seen in figure 15. Because of soil heterogeneity, a sample taken at approximately the same GPS coordinates in March might actually be different enough from soil taken in a slightly different location in October, that the change in [Ti] is more determined by natural soil variation than by basalt addition.

Although samples were taken within roughly 5m of one another each time, only a single- or double-point sample was collected. Then, a small fraction of the sample is used for sample analysis so only a tiny snapshot is captured and not necessarily representative of the site. The unexpected [Ti] can likely be attributed to sampling bias.

Cations

As seen in figures 17, 19, and 21, cation concentration at a given sample location often did not fall within the expected range. Similar to Ti, this is likely due to natural heterogeneity within the field. $\Delta^*[\text{X}]$ shown in figures 16, 18, and 20 provides an indication of how well measured values align with expected values. A value of 0 would mean that the measured value is the same as the expected value. Larger values indicate greater discrepancy.

When averaged across all points within a plot though, cation dissolution did generally follow the expected trend. Table 6 suggests that 73% of the calcium expected to be added as a result of basalt application in plot B (25 t/ha) dissolved within 6 months after basalt application. Similarly, 23% of Mg and 15% of Na is suggested to have dissolved. There was a greater percent dissolution in the lower application plot which is as expected because if both the high application and low application plot are weathering at the same rate, roughly the same concentration of cations will be weathered within the same timeframe but will represent a greater percentage of the lower application rate, compared to the higher application.

A one-way Anova comparing cation dissolution between plots did not show a statistically significant difference, likely as a result of natural variation washing out the signal from basalt. When dissolution was extrapolated across the field, giving a value of cation loss (mol/ha), however, there was a statistically significant difference in Ca loss between plots. More calcium was lost in the highest application rate, compared to the lower application, and more calcium was lost in the lower application rate, compared to the control.

While these results indicate ERW leading to CDR, higher resolution sampling is necessary to more accurately and precisely constrain change in cation dissolution, and therefore CDR rates.

Redesigned sampling plan to capture signal from ERW

Figure 24 provides a theoretical framework, based on the central limit theorem, to understand the extent to which the average of a given number of cores will result in a replicable value, when the mean values of the cores is taken. The mean can be taken either by mechanically homogenizing the individual cores before running analysis (as will be done in this sampling regime), or by running analysis on each sample, and calculating the mean. Analyzing each soil core would be time- and cost-prohibitive in terms of labor and use of the ICP-MS analyzer.

With more soil cores in a sample, the value of the composite sample will more tightly converge around the same value as a different composite sample taken within the same sample radius. If many single- or double-core samples were taken in the same sample radius their values are *not* predicted to be normally distributed around a “true mean.” So, the value of any given sample cannot be taken to be representative of the sample area. This can be seen by the wide spread of data shown in the bottom graph of figure 24, at low values of number of cores in pooled sample. The data shown in the bottom graph of figure 24 is taken from the spread of Δ^* [Ti] seen in the soil samples. The data was normalized so that the mean value = 0.

With 20 cores pooled together into a single sample the value of the pooled sample is expected to be replicable in the sense that if many 20-core samples were taken in the same sample radius, their values would be normally distributed around a “true mean,” as shown in figure 24. The “true mean,” in this case, is the mean that would be found if the entire field was sampled, and the average was taken. This is of course impossible because it would require infinite samples. So, the aim is to determine the number of samples that approaches the “true mean,” with reasonable precision. Different soil properties have different coefficients of variation meaning they are predicted to have different levels of variation across a field, so a different number of samples will be needed to accurately capture different soil properties. This methodology must be validated through implementation in field trials.

The entire 70m x 70m sample plot can be thought of as one sample zone, and the sixteen samples pooled together should start to converge around a “true mean”. This approach was used, for example, in comparing mean [Ca] loss. Any given point on its own, though, cannot provide useful information. Moreover, it is evident that there is significant variation across the 0.49ha plot so higher resolution data is needed to read a signal from basalt over natural soil variation. Thus, a new sampling regime is being implemented to collect and pool 20 soil cores at each sample location, so that any given sample should yield a result that is representative of the sample zone, within approximately a 3m radius. Then, the 16 pooled samples across the sample plot should provide a representative picture of the field.

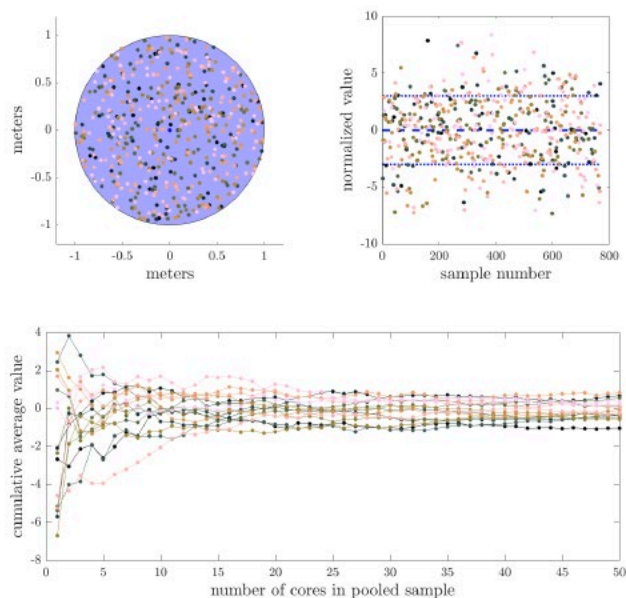


Figure 24: Sensitivity of data distribution as a function of the number of cores in pooled sample. Figure. Figure by Jake Jordan.

Carbon Dioxide Removal

Despite disagreement between expected and measured soil TiCat data, a rough estimate of carbon dioxide removal can still be calculated. The results are on the high end of the CDR estimates found in the literature, but within reasonable range of results from similar setups (see table 9). This information is useful for indicating that weathering is occurring and leading to carbon capture. This data does not yet, however, provide a measurable, reportable, and verifiable quantity of CO₂ sequestration.

Value (1) for CDR in table 8 was calculated based on the TiCat framework, excluding data points that showed a loss in Ti, but including all other data points, regardless of if they fit in the predicted mixing model.

In value (2), negative CDR calculations were removed because elevated cation concentrations, compared to the concentration predicted by the mixing model, is a violation of mass balance as theorized by the TiCAT framework. Increased cation concentration could mean that there was secondary precipitation after weathering, that a third component (i.e. soil from a different part of the field) was introduced to the sample or, most likely, that the post-application sample was taken from a slightly different location than the baseline sample, and the change in cation concentration represents natural variation between the points in the field, rather than weathering.

To calculate value (3), a larger “resampled” data set was created based on the spread of data seen in measured values. First, a subset of data was selected from the overall data—points that did not show a decrease in [Ti] because that would violate conservation of mass as presumed by the TiCat framework. In addition, one other point was removed because the [Mg] concentration was

anomalously high, compared to all other data point which fell within a single standard deviation for the mean [Mg]. Then, a randomized data set was created that has the same mean and standard deviation of the empirical data. The same CDR calculation could then be performed using the mean cation loss of the resampled data. The resulting CDR is well-aligned with the expected CDR, based on data in the literature, and indicates that with more robust sampling and therefore a larger empirical dataset, the TiCat framework could lead to precise CDR measurements.

All CDR calculations assume that the basalt feedstock was spread at exactly the intended application rate (25 t/ha or 7 t/ha) in a uniform sheet across the amended field. It also assumes that there is constant density of the soil and basalt, and the basalt is completely and uniformly mixed with the top 10 cm of soil through tilling.

It is also important to note that CDR values calculated from cation loss in the soil provides an upper bound estimate for actual carbon dioxide removal because CDR is not measured directly but extrapolated from cation loss. In order to use cation loss as a proxy for CDR, the following assumptions must be made:

- 1) 100% of cation loss is due to rock reacting with carbonic acid (that is a product of H₂O and atmospheric CO₂) to produce bicarbonate and dissolved cations which are transported out of the field in aqueous solution.
- 2) The resulting bicarbonate is transported to the ocean and does not precipitate and reemit as CO₂ at any point along the way. Once in the ocean, the bicarbonate sinks below the surface water and either stays as bicarbonate or forms CaCO₃ deep enough that it will not go forward with reaction to reemit CO₂.

Assumption (1) is reasonable in soils with pH close to neutral, as the soils in this study are, because there is not substantial strong acid already in the soil to react with the rock. However, in conventional cropping systems, it is common to allow soil pH to drop below 6 as a result of nitrogen fertilizer (Fernández and Hoefl 2009). In this case, when carbonate or silicate minerals are applied to neutralize soil pH, the rock will likely react with nitric acid in the soil. Dietzen et al suggest that in soils with a baseline pH below 6.3, reactions with other acids must be accounted for in estimating CDR from enhanced weathering. There are methods to account for this, such as estimating concentration of nitric and/or sulfuric acid in the soil, predicting what concentration of strong acid would react with the rock, and subtracting that quantity from the cation loss concentration used to calculate CDR. In soils with a baseline pH below 5.2, ERW may not be an effective CDR technology (Dietzen and Rosing 2023). In addition, cations could be lost to adsorption, mineralization, plant uptake, evapotranspiration, and/or preferential flow, without reacting with atmospheric CO₂ (Amann et al. 2020). Ignoring these other potential mechanisms of cation loss leads to over-estimates of CDR.

In the case of calcium carbonate, or agricultural lime, reaction with nitric acid can lead to net CO₂ emissions because the reaction with nitric acid liberates carbon from the rock and releases it as gaseous CO₂ (West and McBride 2005). In the case of silicate rocks, reaction with nitric acid would not release carbon from the rock, but it also would not capture CO₂, and may lead to a net source of emissions depending on the lifecycle analysis of basalt deployment. In addition, it is possible that addition of silicate-based rocks could increase soil CO₂ emissions (Yan 2023).

Further research is needed to understand the interactions between enhanced rock weathering in soils and soil organic carbon.

It is nearly impossible that 100% of CO₂ that is converted to bicarbonate in the weathering reaction will remain as stable bicarbonate for 1,000+ years, without reemitting as CO₂. So, assumption (2) must be accounted for by integrating models to predict CO₂ leakage after weathering has occurred. Geochemical and hydrological processes predict that dissolved bicarbonate will be transported out of the field either through surface runoff, leaching, or drainage tile. Increase in bicarbonate concentration in watersheds with high agricultural intensity has been observed as a result of agricultural liming (Raymond et al. 2008; Oh and Raymond 2006). This is evidence of effective transport of bicarbonate as a result of rock weathering. However, assumption (2) continues to be a significant unknown in accurately predicting the long-term carbon storage potential of ERW, especially given the high number of variables that could potentially lead to precipitation and reemission between field to ocean (Calabrese et al. 2022). Watershed capacity must be evaluated to ensure that local watersheds do not become oversaturated and in turn reemit the captured CO₂ (Zhang et al. 2022). Further research is needed to understand where dissolved cations go, whether they precipitate, and on what timescales.

Author et al.	Year	Method	Application rate	CDR estimate
Reershemius	2023	Mesocosm	50 t basalt ha ⁻¹	1.06 +- 0.50 tCO ₂ eq ha ⁻¹ , 235 days
Dietzen	2023	Field: Acidic, sandy soil in Denmark, 3 years	50 t Greenlandic glacial rock flour ha ⁻¹	728 kg CO ₂ ha ⁻¹ over 3 years
Buckingham	2022	Mesocosm	100 t basalt ha ⁻¹	0.2 ± 0.8 kgCO ₂ ha ⁻¹ yr ⁻¹
Kelland	2022	Mesocosm	100 t basalt ha ⁻¹	2000 kgCO ₂ ha ⁻¹ yr ⁻¹
Vienne	2022	Mesocosm	50 t basalt ha ⁻¹	1830 kgCO ₂ ha ⁻¹ yr ⁻¹
Kanzaki	2022	Reactive transport model	40 t basalt ha ⁻¹	2-6 tCO ₂ ha ⁻¹ yr ⁻¹
Amann	2020	Mesocosm	242.508 t olivine-rich dunite ha ⁻¹ in the top layer of the soils	0.023–0.049 tCO ₂ @ ha ⁻¹
Taylor	2021	Acid-rain-impacted forested watershed in New Hampshire	3.44 t ha ⁻¹ wollastonite treatment	0.025–0.12 tCO ₂ ha ⁻¹ over 15 years

Lewis	2021	Mineralogy	50 t ha ⁻¹ basalt Australian Tichum	1.3 and 8.5 t CO ₂ (dep on rock type) ha ⁻¹ after 15 years
Haque	202	Leafy vegetable farm, pH = 6.5	1.24 t·hectare ⁻¹ , Wallostonie, 15- 18cm till, irrigated	2.35 t Co ₂ ha ⁻¹ yr ⁻¹ (based on SIC content)
Strefler	2018	Model	pH of 7 and temperature of 25 °C	Basalt: 10 ^{·10.53} mol m ⁻² s ⁻¹ Dunite: 10 ^{·9.86} mol m ⁻² s ⁻¹

Table 9: CDR as a result of ERW reported in the literature

Section 4: Carbon Budget

Methods

Carbon Cycle

Carbon fluxes in agricultural settings are governed by both natural processes and external (i.e., human-induced) inputs.

The gross uptake of CO₂ via photosynthesis is known as gross primary production (GPP). About half of this photo-assimilated carbon is released back into the atmosphere via autotrophic respiration (R_a). The relationship between GPP and R_a describes an ecosystem's net primary production (NPP). NPP relates to GPP and R_a as $NPP = GPP - R_a$. While the majority of NPP is assigned to the production of above- and below-ground biomass, it is near impossible to get an accurate measurement of total NPP due to exudation from roots, emission of volatile organic compounds, carbon transfer to root symbionts and losses of biomass due to pests or herbivory. These unknown fractions are never included in a budget; therefore, an underestimation is built into the system.

Soil organic carbon (SOC) refers to a pool of carbon stored in the soil that results from plant matter and other carbon-based life that has died. Organic carbon is subject to microbial decomposition, by which carbon is released back into the atmosphere. This process is known as heterotrophic respiration (R_h). The total sum of ecosystem respiration (R_e) is found by adding R_h and R_a, and the difference between GPP and R_e is known as net ecosystem productivity (NEP) and is represented as: $NEP = GPP - R_e$ or $NEP = NPP - R_h$

Natural rock weathering does not contribute a significant carbon flux in our agricultural field because it occurs at a very slow rate in comparison to the other carbon fluxes accounted for. Enhanced rock weathering speeds up this process, such that it has a significant impact on carbon cycling.

Existing literature on carbon and greenhouse gas emissions in soy/corn cropping systems was compiled and extrapolated for the test site at Zumwalt Acres, in addition to empirical data collected on-site. Most studies used the Eddy Covariance (EC) method and simulated models. The EC method measure carbon, water, and heat flows between plant communities and the atmosphere directly (Baldocchi 1988; Verma 1989; Kaimal 1994; Lee 2004; Liang 2012; Burba 2013).

Soil stock

A soil stock of 523,777 g C/m² in the top 10cm of soil was calculated based on 2.57% soil organic carbon in the top 10cm and 1.36 g/cm³ soil bulk density. Percent soil organic carbon was calculated based on the average loss of ignition from all samples (calculated based on the difference in mass of dried sampling before after ashing) and the linear regression $SOC = 0.6094 * LOI + 0.1949$ (Konen et al. 2002).

Total inorganic carbon (TIC) was measured on soil samples taken at Zumwalt Acres in Site #5 in 2021 and showed 0% TIC detected. A similar field site in Champaign, IL also showed 0% TIC in

control and basalt-treated corn/soy fields. So, it is assumed that total inorganic carbon in Site #1 is also negligible.

GPP and Ecosystem Respiration

To calculate GPP and ecosystem respiration, average values were taken from data found in the literature (see appendix for full carbon budget and sources). Each of these studies focused on analogue cropping systems and were relatively in agreement with a standard deviation of 10% for GPP and 13% for ecosystem respiration for corn. Less data was available on soy, and the standard deviation was 15% and 34% respectively. GPP is estimated to be -1492 gC/m² for corn and -931 gC/m² for soy. Re is estimated to be 1075 gC/m² for corn and 905 gC/m² for soy. To calculate NEP, Re is subtracted from GPP, which results in -417 gC/m² for corn and -850 gC/m² for soy.

Harvest

Grain from the crops will be exported from the ecosystem and sold at market, eventually going back into the cycle somewhere else. Corn silage and bean plant residue was assumed to be left on the field such that only the grain/beans are exported. Based on previous studies and USDA yield data, the average value of carbon in exported crops was calculated. Again, each study was in close agreement. A net ecosystem carbon balance (NECB) of 191 gCE/m² for corn and 157 gCE/m² for soy was calculated, based on NEP and harvest data. This is in alignment with similar studies reported in the literature (Eichmann 2016; Zeri 2011).

Additional inputs

Production, transportation, storage, and application of fertilizers and herbicides contribute to the overall carbon budget, as does on-farm machinery use. R. Lal's paper, "Carbon Emission From Farm Operations" was used for estimates of external fluxes. These fluxes, in comparison to internal fluxes, are relatively small, so exact accuracy was not necessary to understand a broad picture of the carbon budget. Actual management practices on the field site at Zumwalt Acres informed the construction of the budget. The full list of external inputs with application rates with more specific associated emissions can be found in the appendix.

The total sum of machinery usage amounts to 7.8 gCE/m² for corn and 3.7 gCE/m² for soy. The sum production, transportation, and storage of various agrochemicals results in 116 gCE/m² for corn and 18 gCE/m² for soy production. Corn has a much higher input value because nitrogen and other fertilizers are used, while no fertilizers are used for a soy crop.

Overall

Including external inputs, neglecting liming or basalt addition, the overall carbon budget is estimated to be 114 gCE/m² for corn and 22 gCE/m² for soy.

Basalt inputs

The energy necessary for mining operations is relatively low, producing 1.6 kg CO₂e/t rock (Strefler 2018). Grinding emissions can range from 3.6 to 116.1 kg CO₂/tonne of rock, depending on the grain size, with emission costs increasing as grain size is reduced (Strefler

2018). The rock is already ground to a powder as a byproduct of the mining process, so little post-processing is needed before farm application.

Transportation is a key factor in assessing a carbon budget for enhanced rock weathering because trucking rock far distances results in significant greenhouse gas emissions. However, the current transportation infrastructure is not necessarily representative of long-term deployment plans. Ideally nearby mines are located to supply farmers and trains or barges are utilized for most of the transportation. The emissions associated with diesel trucking is estimated at 0.0473 kg CO₂e/t rock/km. From Pioneer Valley, Ma, that would result in approximately 50 gC/m². From the Specialty Granule mine in Wisconsin, the emissions would be approximately 27 gC/m².

Liming was not included in the carbon budget because constraining the net carbon emissions or sequestration as a result of liming is out of the scope of this study.

Basalt Carbon Capture

Actual carbon dioxide removal on a one-to-two-year timeline is also not yet well constrained, as discussed in section 3. However, based on data collected in this study and other studies, it is reasonable to assume that CDR ranges from 2-4 tCO₂/ha or 55 – 110 gC/m² within one year after application.

Discussion

Constructing carbon budgets can be useful for understanding carbon cycling within the entire system of interest. Especially in considering negative emissions technologies, it is essential to ensure that the process that is intended to remove carbon from the atmosphere does not in turn emit significant carbon, at a different point in the life cycle. It is also useful to compare negative emissions technologies to baseline emissions, to understand the potential scale of impact.

It can be seen from this budget that whether ERW results in negative emissions in a given year is dependent on crop type, as well as management practices. Carbon cycling in agricultural settings is largely governed by internal fluxes—carbon moving through the soil, plants, and atmosphere. The extent of CDR (~100 gC/m²) is commensurate to the carbon emissions associated with external fluxes (~115 gC/m² from machinery, fertilizers, and herbicides). This budget suggests that if basalt is acquired from a nearby mine and/or transported by rail, ERW could approximately offset the CO₂ emissions associated with external inputs in conventional cropping systems in the Midwest. As agriculture contributes 10% of global greenhouse gas emissions, offsetting these emissions could substantially impact global atmospheric CO₂ concentration (US EPA).

That said, in constructing a carbon budget for an agricultural field, there are numerous uncertainties. Data on life cycle analysis from the specific agricultural inputs used in each site is limited. Small differences within this test site and between this site and the test sites from which data was pulled can amount to significant differences in carbon calculations.

This budget was tailored to a two-year timeframe, a relatively small plot with mostly consistent soil texture, and to a soil depth of 0.1m. A carbon budget represents a snapshot of potential carbon fluxes and pools at a given time. There is seasonal variation in soil carbon stocks and

ecosystem respiration based on changes in temperature and precipitation and of course, at different points in the year, machinery use and human inputs and outputs vary significantly. From year to year, soil changes and management practices change.

Moreover, enhanced rock weathering is predicted to have long-term effects in terms of inorganic carbon sequestration, soil organic carbon, above ground biomass, and soil emissions (Lewis 2021; Yan 2023).

In tabulating values for carbon emissions associated with production, transportation, storage and transfer of chemicals, the exact values for each product used in our test site were not available. Aggregate data was used, comparing multiple sources, and selecting for management and environmental conditions that mostly closely aligned with this test site.

While important to consider life cycle emissions associated with basalt mining, grinding, and transportation, when the basalt is acquired as a waste product, the calculation in a life cycle assessment is different. It is useful to compare life cycle emissions of basalt versus limestone in each farm context, as limestone is a baseline practice for farmers to achieve neutralize soil pH. Limestone is often mined specifically for agricultural purposes, while the basalt used was a byproduct that would have been mined anyway, as part of the shingles industry. In Illinois though, lime quarries are as little as 10km away, while basalt mines are 100s of kms away. If carbon emissions associated with basalt deployment is greater than limestone, it is essential to assess if there is still meaningful net CDR.

Additionally, studies show that grain size is directly related to the annual carbon dioxide removal (CDR) potential and is also related to the overall energy required to produce ideal ultrafine particles ($50\mu\text{m} - 2\mu\text{m}$). There is a balance between grain size, CDR potential, and cost effectiveness (Lewis 2021; Rinder 2021).

As described, estimates for carbon capture as a result of enhanced rock weathering are not yet well constrained. At $55 - 110 \text{ gC/m}^2$ though, the predicted ERW CDR rate is within the same range as emissions resulting from external fluxes associated with conventional agriculture (e.g., machinery, fertilizers, herbicides). So, ERW could potentially offset emissions associated with conventional agriculture, which is significant at 10% of the global greenhouse gas emissions budget (US EPA).

A combination of more refined models and significantly more on-farm field trial data is needed to confidently predict the amount of carbon captured per area, given a specific basalt application rate, in one year and over time. These estimates must also be geographically and temporally constrained. Water flux, soil organic matter, tillage depth, timing of tilling in comparison to basalt application, type of basalt used, particle size of basalt, are all factors that influence how much carbon will be sequestered. Due to different rates of weathering of different minerals in a given basalt, carbon capture rates vary year to year and the full potential of capture is not realized for decades or longer. This makes it difficult to constrain a yearly capture rate. It is important to note that, as opposed to the carbon flux associated with pesticide application for example, the carbon flux associated with basalt must consider the site history—if basalt had been

applied the year prior, the next carbon flux due to basalt will be different than if basalt is being applied for the first time.

Management decisions cannot be based on carbon emissions alone but must consider the wide scope of environmental, social, and economic factors involved. Moreover, carbon capture solutions, such as enhanced rock weathering, will not significantly reduce climate change, without the simultaneous decarbonization of our economy. Whether discussing ERW, direct air carbon capture, afforestation, or other mechanisms of carbon drawdown, all these systems rely on fossil fuels to implement the solution. Therefore, it is a losing battle to achieve negative emissions. Still, carbon capture solutions need to be investigated so that, as we decarbonize the energy sector, we can also implement negative emissions to avoid the worst effects of climate change.

Conclusion

This study provides crucial insight into how field trials should be designed to provide empirical data on the effectiveness of enhanced rock weathering to mitigate climate change and improve agricultural resiliency. Six months after application, average pH remained around neutral in both control and test plots. Yields were increased or remained unaffected by basalt. The data was insufficient to make definite claims about the effect of weathering on change in soil cation concentration, and therefore to calculate CDR with reasonable accuracy and precision. That said, the data provides indication of CDR and reason to believe that with more robust sampling, we could calculate weathering rates with accuracy and precision that align with previous studies reported in the literature. This study provides key information about the type of sampling that would allow us to do those calculations with confidence.

Further research that integrates learnings from this study will output science that either underpins or debunks the merit of ERW deployment in the American corn belt as a net positive for farmers, ecosystems, and all humans in the face of climate change. It will not, however, provide a framework for corporations to mint carbon credits on a tons-CO₂-captured basis, as other monitoring, reporting, and verification studies seek to do because methodology to determine long-term CO₂ sequestration (needed to reasonably claim CO₂ offsets) have not yet been developed.

Other considerations

There are many important factors impacting the potential of enhanced rock weathering that are not specifically discussed in this report. For example, other potential risks include heavy metal contamination and dust production.

ERW could have synergistic effects with some other regenerative agriculture practices but is incompatible with others. Practices that increase soil water holding capacity and microbial processes can accelerate ERW even further, especially by stimulating arbuscular mycorrhizal fungi (verbruggen 2021). On the other hand, ERW should not be deployed with no-till, one of the most prevalent conservation agricultural practices used today (Chen 2022). No-till farming can reduce soil erosion (seitz 2020). However, if basalt is not mixed with the soil, it is more likely to be washed off the field without achieving the intended benefits.

ERW has primarily only been studied in field trials on major cash crops and on bioenergy crops, but different crops respond differently to basalt application, especially at heavy rates. A shift towards diversified agriculture should be taken into consideration in a basalt roll-out, as diversified systems improve farmers economic resilience and strengthens local foodsheds. ERW is challenging in perennial systems because the machinery needed to apply and till basalt in is generally incompatible with perennial systems. However, enhanced rock weathering can, and has, been used in forested landscapes, and perennial systems should be included within the scope of ERW study.

Next Steps

Sampling

Beginning this spring the redesigned sampling plan is being implemented to allow for more robust elemental data, and accordingly, more robust CDR estimates. A new site has received basalt treatment this spring and a corresponding control plot was established. This site and existing sites will be analyzed according to the new sampling plan, allowing for multi-year monitoring.

An Eijkelkamp grass plot sampler - 0.9-inch is being used, rather than the previous AMS sampler, which reduced the time and labor associated with sampling, but only allows for samples at 0-10cm. Instead of each sample being composed of a single or double core, 20 samples are taken at each GPS location and homogenized to make a single sample. The samples are taken within a 3m radius, with 5 samples taken in random locations in each quadrant of the circle.

In addition, in each sampling plot, two points are used for high-resolution augmented sampling. In high-resolution augment samples, 20 samples with an increasing number of soil cores are taken within the 3m-radius sample circle: the first sample is one soil core, the second sample is comprised of two soil cores, the third sample is comprised of three soil cores and so on until the twentieth which is comprised of 20 soil cores. Soil cores in pooled samples are homogenized as thoroughly as possible.

In addition, in each plot, two points are used for low-resolution augmented sampling. The same procedure is repeated but only four samples are taken per point—a single core sample, 5-core sample, 10-core sample, and 20-core sample.

Augmented samples will be used to identify how many samples, on average, are needed to get data that converge around a representative value of the soil in that area.

Soil Health

Biological factors are a key component of the weathering process, but the interactions are not well understood (Vicca 2021; Rebeiro 2020). Fungal contribution to natural silicate weathering rates in soil has been studied and is beginning to be studied in the context of enhanced weathering, finding that fungi colonization plays a significant role in weathering rates (Wild 2021; Burghelea 2015; Quirk 2012).

In addition to the existing sample analysis procedures, soil health and plant tissue analysis is being implemented beginning this spring, in collaboration with Dr. Maria Bonita Villamil and Dr. Esther Ngumbi at University of Illinois in Urbana Champaign. On a subset of the same soil samples phospholipid-derived fatty acid analysis will be conducted to understand broadly the change in community composition of soil microbiota in response to basalt addition. Potentially mineralizable nitrogen, total nitrogen, active carbon, total organic carbon, wet aggregate stability, pH (salt and water), effective cation exchange capacity, effective base saturation, and plant available phosphorus will also be measured. These tests will be conducted at the University of Missouri External Soil Health Assessment Center.

We will collect plant samples at three sampling times during the growing season (at two, four, and eight weeks after planting in the spring and summer of 2023). Plant health metrics will be analyzed through targeted secondary metabolite profiling in plant roots and shoots using Ultra High Performance Liquid Chromatography - Mass Spectroscopy - (UHPLC-MS) at the Metabolome center at University of Illinois.

Looking Forward: Deployment

Leading scientists advocate for ERW deployment in agricultural settings across millions of hectares of farmland, leading to potentially gigatons of CO₂ removal from the atmosphere (Kanzatas 2022; Beerling 2020; Strefler 2018). In the last three years, dozens of startups have begun implementing ERW across hundreds of hectares of farmland, financed through carbon credits (e.g. Lithos Carbon, Undo, Project Vesta, The Future Forest Company). This rapid scaling is due, at least in part, to investments by large corporations including FedEx, Boeing, Stripe, Microsoft, and others looking to identify pathways towards offsetting their carbon emissions.

Negative emissions technologies are essential to help ensure resilient ecosystems, even if we were to entirely halt greenhouse gas emissions today, and carbon credits are one way to fund these technologies in the near-term. The longer we wait to reduce atmospheric carbon dioxide, the worse the consequences will be due to climate feedbacks.

As of January 2023, the global monthly mean CO₂ concentration was 419.31 ppm, a 20% increase since 1980. Even under the most optimistic predictions by the Intergovernmental Panel on Climate Change (SSP1-1.9), CO₂ concentration is predicted to rise to 425.53 by 2040 leading to a 1.56°C mean temperature increase (US Department). That means that within the next two decades will almost surely exceed what is considered a critical temperature threshold (1.5 °C) in terms of consequences on human quality of life. Moreover, SSP1 would require a tremendous shift in global political cooperation, substantial degrowth, especially by large corporations, and a significant lifestyle change, especially by the upper class.

For many corporations, cutting emissions without shutting down, scaling down, or changing the services they provide, is nearly impossible. Low-emissions technologies that can provide comparable services to such companies' existing technologies are far from available.

So, corporations are investing in technologies that are expected to be effective, scalable, and affordable methods of carbon drawdown to compensate for their continual emissions. This may be motivated, at least in part, in anticipation of potential government mandates limiting emissions or requiring offsets.

Sometimes carbon offset initiatives are paired with commitments from the corporations to cut their emissions as well (e.g. FedEx). In large part though, carbon offset initiatives are designed to allow the corporation to continue to operate as they have been, while avoiding legal restrictions, despite the known negative global consequences of their resulting emissions.

Agricultural ERW is a prime option for carbon offset programs because it is well-suited to plug into existing infrastructure, politics, and economics. If material acquisition, transportation, and

spreading is well-designed, all the needed infrastructure can be readily available, especially in regions where farmers typically apply limestone. ERW also is not subject to the same criticism of impermanence as organic carbon capture strategies such as no-till agriculture and afforestation. However, premature carbon markets have arisen, that are not sufficiently backed by scientific evidence, to ensure meaningful carbon sequestration. Moreover, carbon markets allow large corporations to continue to profit, while placing undo burden on low-income communities and communities of color (Lejano 2020; Schlosberg 2014). In envisioning a climate resilient future, carbon-drawdown strategies must be implemented in a way that alleviates burden from communities already facing environmental injustice and holds the largest emitters accountable.

ERW could play a critical role in averting the worst effects of climate change and improving agriculture. But, before rolling out deployment on a million-hectare scale, it will be essential that the scientific questions have been answered within reasonable and known uncertainty, and the sociopolitical considerations have been addressed. Who is bearing the risk and who is reaping the benefits, today and seven generations¹ from now?

¹ The seventh generation principle is a core value of Haudenosaunee people that says that decisions made today should take into account the impacts they will have on generations to come.

References

- Ab Manan, Wan. 2018. "Optimization of Soil PH by Using Calcium Carbonate (CaCO₃) Obtained from Seashell Waste," September.
- Almaraz, Maya, Nina L. Bingham, Iris O. Holzer, Emily K. Geoghegan, Heath Goertzen, Jaeun Sohng, and Benjamin Z. Houlton. 2022. "Methods for Determining the CO₂ Removal Capacity of Enhanced Weathering in Agronomic Settings." *Frontiers in Climate* 4. <https://www.frontiersin.org/articles/10.3389/fclim.2022.970429>.
- Almaraz, Maya, Michelle Y. Wong, Emily K. Geoghegan, and Benjamin Z. Houlton. 2021. "A Review of Carbon Farming Impacts on Nitrogen Cycling, Retention, and Loss." *Annals of the New York Academy of Sciences* 1505 (1): 102–17. <https://doi.org/10.1111/nyas.14690>.
- Amann, Thorben, Jens Hartmann, Eric Struyf, Wagner de Oliveira Garcia, Elke K. Fischer, Ivan Janssens, Patrick Meire, and Jonas Schoelynck. 2020. "Enhanced Weathering and Related Element Fluxes – a Cropland Mesocosm Approach." *Biogeosciences* 17 (1): 103–19. <https://doi.org/10.5194/bg-17-103-2020>.
- Andrews, M. Grace, and Lyla L. Taylor. 2019. "Combating Climate Change Through Enhanced Weathering of Agricultural Soils." *Elements* 15 (4): 253–58. <https://doi.org/10.2138/gselements.15.4.253>.
- Beerling, David J., Jonathan R. Leake, Stephen P. Long, Julie D. Scholes, Jurriaan Ton, Paul N. Nelson, Michael Bird, et al. 2018. "Farming with Crops and Rocks to Address Global Climate, Food and Soil Security." *Nature Plants* 4 (3): 138–47. <https://doi.org/10.1038/s41477-018-0108-y>.
- Behnke, Gevan D., and María B. Villamil. 2019. "Cover Crop Rotations Affect Greenhouse Gas Emissions and Crop Production in Illinois, USA." *Field Crops Research* 241 (September): 107580. <https://doi.org/10.1016/j.fcr.2019.107580>.
- Bhat, M. G., B. C. English, A. F. Turhollow, and H. O. Nyangito. 1994. "Energy in Synthetic Fertilizers and Pesticides: Revisited. Final Project Report." ORNL/Sub-90-99732/2. Oak Ridge National Lab. (ORNL), Oak Ridge, TN (United States); Tennessee Univ., Knoxville, TN (United States). Dept. of Agricultural Economics and Rural Sociology. <https://doi.org/10.2172/10120269>.
- Brantley, S. L., Andrew Shaughnessy, Marina I. Lebedeva, and Victor N. Balashov. 2023. "How Temperature-Dependent Silicate Weathering Acts as Earth's Geological Thermostat." *Science* 379 (6630): 382–89. <https://doi.org/10.1126/science.add2922>.
- Brimhall, George H, and William E Dietrich. 1987. "Constitutive Mass Balance Relations between Chemical Composition, Volume, Density, Porosity, and Strain in Metasomatic Hydrochemical Systems: Results on Weathering and Pedogenesis." *Geochimica et Cosmochimica Acta* 51 (3): 567–87. [https://doi.org/10.1016/0016-7037\(87\)90070-6](https://doi.org/10.1016/0016-7037(87)90070-6).
- Buckingham, F. L., G. M. Henderson, P. Holdship, and P. Renforth. 2022. "Soil Core Study Indicates Limited CO₂ Removal by Enhanced Weathering in Dry Croplands in the UK." *Applied Geochemistry* 147 (December): 105482. <https://doi.org/10.1016/j.apgeochem.2022.105482>.
- Burghelea, C., D. G. Zaharescu, K. Dontsova, R. Maier, T. Huxman, and J. Chorover. 2015. "Mineral Nutrient Mobilization by Plants from Rock: Influence of Rock Type and Arbuscular Mycorrhiza." *Biogeochemistry* 124 (1): 187–203. <https://doi.org/10.1007/s10533-015-0092-5>.
- Calabrese, Salvatore, Bastien Wild, Matteo B. Bertagni, Ian C. Bourg, Claire White, Felipe Aburto, Giuseppe Cipolla, Leonardo V. Noto, and Amilcare Porporato. 2022. "Nano- to Global-Scale Uncertainties in Terrestrial Enhanced Weathering." *Environmental Science & Technology* 56 (22): 15261–72. <https://doi.org/10.1021/acs.est.2c03163>.

- Chadwick, Oliver A., George H. Brimhall, and David M. Hendricks. 1990. "From a Black to a Gray Box — a Mass Balance Interpretation of Pedogenesis." *Geomorphology*, Proceedings of the 21st Annual Binghamton Symposium in Geomorphology, 3 (3): 369–90. [https://doi.org/10.1016/0169-555X\(90\)90012-F](https://doi.org/10.1016/0169-555X(90)90012-F).
- Chen, Le, Roderick M. Rejesus, Serkan Aglasan, Stephen Hagen, and William Salas. 2023. "The Impact of No-till on Agricultural Land Values in the United States Midwest." *American Journal of Agricultural Economics* 105 (3): 760–83. <https://doi.org/10.1111/ajae.12338>.
- Conceição, Lucas Terto, Gutierrez Nelson Silva, Heverton Manoel Silva Holsback, Caroline de Figueiredo Oliveira, Nericleas Chaves Marcante, Éder de Souza Martins, Fabio Luís de Souza Santos, and Elcio Ferreira Santos. 2022. "Potential of Basalt Dust to Improve Soil Fertility and Crop Nutrition." *Journal of Agriculture and Food Research* 10 (December): 100443. <https://doi.org/10.1016/j.jafr.2022.100443>.
- Dietzen, Christiana, and Minik T. Rosing. 2023. "Quantification of CO₂ Uptake by Enhanced Weathering of Silicate Minerals Applied to Acidic Soils." *International Journal of Greenhouse Gas Control* 125 (May): 103872. <https://doi.org/10.1016/j.ijggc.2023.103872>.
- Dold, C., K. M. Wacha, T. J. Sauer, J. L. Hatfield, and J. H. Prueger. 2021. "Measured and Simulated Carbon Dynamics in Midwestern U.S. Corn-Soybean Rotations." *Global Biogeochemical Cycles* 35 (1): e2020GB006685. <https://doi.org/10.1029/2020GB006685>.
- Dontsova, Katerina, Zsuzsanna Balogh-Brunstad, and Jon Chorover. 2020. "Plants as Drivers of Rock Weathering." In *Biogeochemical Cycles*, 33–58. American Geophysical Union (AGU). <https://doi.org/10.1002/9781119413332.ch2>.
- Dupla, Xavier, Benjamin Möller, Philippe C. Baveye, and Stéphanie Grand. 2023. "Potential Accumulation of Toxic Trace Elements in Soils during Enhanced Rock Weathering." *European Journal of Soil Science* 74 (1): e13343. <https://doi.org/10.1111/ejss.13343>.
- Eichelmann, Elke, Claudia Wagner-Riddle, Jon Warland, Bill Deen, and Paul Voroney. 2016a. "Comparison of Carbon Budget, Evapotranspiration, and Albedo Effect between the Biofuel Crops Switchgrass and Corn." *Agriculture, Ecosystems & Environment* 231 (September): 271–82. <https://doi.org/10.1016/j.agee.2016.07.007>.
- . 2016b. "Comparison of Carbon Budget, Evapotranspiration, and Albedo Effect between the Biofuel Crops Switchgrass and Corn." *Agriculture, Ecosystems & Environment* 231 (September): 271–82. <https://doi.org/10.1016/j.agee.2016.07.007>.
- Eranki, Pragnya L., Jay Devkota, and Amy E. Landis. 2019. "Carbon Footprint of Corn-Soy-Oats Rotations in the US Midwest Using Data from Real Biological Farm Management Practices." *Journal of Cleaner Production* 210 (February): 170–80. <https://doi.org/10.1016/j.jclepro.2018.11.002>.
- Fernández, Fabián, and Robert Hoefl. 2009. "Managing Soil PH and Crop Nutrients." In *Illinois Agronomy Handbook*. Vol. 8. University of Illinois Department of Crop Sciences.
- "Full Throttle Ag Service." n.d. Longlivesoil. Accessed May 3, 2023. <https://www.longlivesoil.com>.
- Gudbrandsson, Snorri, Domenik Wolff-Boenisch, Sigurdur R. Gislason, and Eric H. Oelkers. 2011. "An Experimental Study of Crystalline Basalt Dissolution from 2 ≤ pH ≤ 11 and Temperatures from 5 to 75°C." *Geochimica et Cosmochimica Acta* 75 (19): 5496–5509. <https://doi.org/10.1016/j.gca.2011.06.035>.
- Hamilton, Stephen K., Amanda L. Kurzman, Clay Arango, Lixin Jin, and G. Philip Robertson. 2007. "Evidence for Carbon Sequestration by Agricultural Liming." *Global Biogeochemical Cycles* 21 (2). <https://doi.org/10.1029/2006GB002738>.

- Hernandez-Ramirez, Guillermo, Jerry L. Hatfield, Timothy B. Parkin, Thomas J. Sauer, and John H. Prueger. 2011. "Carbon Dioxide Fluxes in Corn–Soybean Rotation in the Midwestern U.S.: Inter- and Intra-Annual Variations, and Biophysical Controls." *Agricultural and Forest Meteorology* 151 (12): 1831–42. <https://doi.org/10.1016/j.agrformet.2011.07.017>.
- Huang, Yao, Yongqiang Yu, Wen Zhang, Wenjuan Sun, Shiliang Liu, Jun Jiang, Jinshui Wu, Wantai Yu, Yu Wang, and Zhaofang Yang. 2009. "Agro-C: A Biogeophysical Model for Simulating the Carbon Budget of Agroecosystems." *Agricultural and Forest Meteorology* 149 (1): 106–29. <https://doi.org/10.1016/j.agrformet.2008.07.013>.
- Inagaki, Thiago Massao, João Carlos de Moraes Sá, Eduardo Fávero Caires, and Daniel Ruiz Potma Gonçalves. 2016. "Lime and Gypsum Application Increases Biological Activity, Carbon Pools, and Agronomic Productivity in Highly Weathered Soil." *Agriculture, Ecosystems & Environment* 231 (September): 156–65. <https://doi.org/10.1016/j.agee.2016.06.034>.
- IPCC. n.d. "FAQ Chapter 4 — Global Warming of 1.5 °C." Accessed April 30, 2023. <https://www.ipcc.ch/sr15/faq/faq-chapter-4/>.
- Jansson, Janet K., and Kirsten S. Hofmockel. 2020. "Soil Microbiomes and Climate Change." *Nature Reviews Microbiology* 18 (1): 35–46. <https://doi.org/10.1038/s41579-019-0265-7>.
- Kantzas, Euripides P., Maria Val Martin, Mark R. Lomas, Rafael M. Eufrazio, Phil Renforth, Amy L. Lewis, Lyla L. Taylor, et al. 2022. "Substantial Carbon Drawdown Potential from Enhanced Rock Weathering in the United Kingdom." *Nature Geoscience* 15 (5): 382–89. <https://doi.org/10.1038/s41561-022-00925-2>.
- Konen, Michael E., Peter M. Jacobs, C. Lee Burras, Brandi J. Talaga, and Joseph A. Mason. 2002. "Equations for Predicting Soil Organic Carbon Using Loss-on-Ignition for North Central U.S. Soils." *Soil Science Society of America Journal* 66 (6): 1878–81. <https://doi.org/10.2136/sssaj2002.1878>.
- Kool, A, M Marinussen, H Blonk, and Blonk Consultants. n.d. "LCI Data for the Calculation Tool Feedprint for Greenhouse Gas Emissions of Feed Production and Utilization."
- Lal, R. 2004. "Carbon Emission from Farm Operations." *Environment International* 30 (7): 981–90. <https://doi.org/10.1016/j.envint.2004.03.005>.
- Landis, Amy E., Shelie A. Miller, and Thomas L. Theis. 2007. "Life Cycle of the Corn–Soybean Agroecosystem for Biobased Production." *Environmental Science & Technology* 41 (4): 1457–64. <https://doi.org/10.1021/es0606125>.
- Lejano, Raul P., Wing Shan Kan, and Ching Chit Chau. 2020. "The Hidden Disequities of Carbon Trading: Carbon Emissions, Air Toxics, and Environmental Justice." *Frontiers in Environmental Science* 8. <https://www.frontiersin.org/articles/10.3389/fenvs.2020.593014>.
- Lewis, Amy L., Binoy Sarkar, Peter Wade, Simon J. Kemp, Mark E. Hodson, Lyla L. Taylor, Kok Loong Yeong, et al. 2021. "Effects of Mineralogy, Chemistry and Physical Properties of Basalts on Carbon Capture Potential and Plant-Nutrient Element Release via Enhanced Weathering." *Applied Geochemistry* 132 (September): 105023. <https://doi.org/10.1016/j.apgeochem.2021.105023>.
- Oh, Neung-Hwan, and Peter A. Raymond. 2006. "Contribution of Agricultural Liming to Riverine Bicarbonate Export and CO₂ Sequestration in the Ohio River Basin." *Global Biogeochemical Cycles* 20 (3). <https://doi.org/10.1029/2005GB002565>.
- Patel, M., A. Theiss, and E. Worrell. 1999. "Surfactant Production and Use in Germany: Resource Requirements and CO₂ Emissions." *Resources Conservation and Recycling*. <https://www.semanticscholar.org/paper/Surfactant-production-and-use-in-Germany%3A-resource-Patel-Theiss/33c8d2960542c1c5659a3050a86eeab3a1074d26>.

- Paustian, Keith, Mark Easter, Kevin Brown, Adam Chambers, Marlen Eve, Adriane Huber, Ernie Marx, et al. 2017. "Field- and Farm-Scale Assessment of Soil Greenhouse Gas Mitigation Using COMET-Farm." In *Precision Conservation: Geospatial Techniques for Agricultural and Natural Resources Conservation*, 341–59. John Wiley & Sons, Ltd.
<https://doi.org/10.2134/agronmonogr59.c16>.
- Pogge von Strandmann, Philip, Chloe Tooley, Josephine Mulders, and Phil Renforth. n.d. "Frontiers | The Dissolution of Olivine Added to Soil at 4°C: Implications for Enhanced Weathering in Cold Regions." Accessed May 4, 2023.
<https://www.frontiersin.org/articles/10.3389/fclim.2022.827698/full>.
- Quirk, Joe, David J. Beerling, Steve A. Banwart, Gabriella Kakonyi, Maria E. Romero-Gonzalez, and Jonathan R. Leake. 2012. "Evolution of Trees and Mycorrhizal Fungi Intensifies Silicate Mineral Weathering." *Biology Letters* 8 (6): 1006–11. <https://doi.org/10.1098/rsbl.2012.0503>.
- Raymond, Peter A., Neung-Hwan Oh, R. Eugene Turner, and Whitney Broussard. 2008. "Anthropogenically Enhanced Fluxes of Water and Carbon from the Mississippi River." *Nature* 451 (7177): 449–52. <https://doi.org/10.1038/nature06505>.
- Ribeiro, Igor Daniel Alves, Camila Gazolla Volpiano, Luciano Kayser Vargas, Camille Eichelberger Granada, Bruno Brito Lisboa, and Luciane Maria Pereira Passaglia. 2020a. "Use of Mineral Weathering Bacteria to Enhance Nutrient Availability in Crops: A Review." *Frontiers in Plant Science* 11. <https://www.frontiersin.org/articles/10.3389/fpls.2020.590774>.
- . 2020b. "Use of Mineral Weathering Bacteria to Enhance Nutrient Availability in Crops: A Review." *Frontiers in Plant Science* 11.
<https://www.frontiersin.org/articles/10.3389/fpls.2020.590774>.
- Rinder, Thomas, and Christoph von Hagke. 2021. "The Influence of Particle Size on the Potential of Enhanced Basalt Weathering for Carbon Dioxide Removal - Insights from a Regional Assessment." *Journal of Cleaner Production* 315 (September): 128178.
<https://doi.org/10.1016/j.jclepro.2021.128178>.
- Schlosberg, David, and Lisette B. Collins. 2014. "From Environmental to Climate Justice: Climate Change and the Discourse of Environmental Justice." *WIREs Climate Change* 5 (3): 359–74.
<https://doi.org/10.1002/wcc.275>.
- Seitz, Steffen, Volker Prasuhn, and Thomas Scholten. 2020. "Controlling Soil Erosion Using No-Till Farming Systems." In *No-till Farming Systems for Sustainable Agriculture: Challenges and Opportunities*, edited by Yash P. Dang, Ram C. Dalal, and Neal W. Menzies, 195–211. Cham: Springer International Publishing. https://doi.org/10.1007/978-3-030-46409-7_12.
- Sikora, F. J. 2006. "A Buffer That Mimics the SMP Buffer for Determining Lime Requirement of Soil." *Soil Science Society of America Journal* 70 (2): 474–86.
<https://doi.org/10.2136/sssaj2005.0164>.
- Smith, Douglas R., Kevin W. King, Laura Johnson, Wendy Francesconi, Pete Richards, Dave Baker, and Andrew N. Sharpley. 2015. "Surface Runoff and Tile Drainage Transport of Phosphorus in the Midwestern United States." *Journal of Environmental Quality* 44 (2): 495–502.
<https://doi.org/10.2134/jeq2014.04.0176>.
- Soil Survey Staff. 2022. "Kellogg Soil Survey Laboratory Methods Manual." Soil Survey Investigations 42, Version 6. Part 1: Current Methods. United States Department of Agriculture, Natural Resource Conservation Service.
- Son, Yejin, Kevin Stott, David A. C. Manning, and Julia M. Cooper. 2021. "Carbon Sequestration in Artificial Silicate Soils Facilitated by Arbuscular Mycorrhizal Fungi and Glomalin-Related Soil Protein." *European Journal of Soil Science* 72 (2): 863–70. <https://doi.org/10.1111/ejss.13058>.

- Strefler, Jessica, Thorben Amann, Nico Bauer, Elmar Kriegler, and Jens Hartmann. 2018. "Potential and Costs of Carbon Dioxide Removal by Enhanced Weathering of Rocks." *Environmental Research Letters* 13 (3): 034010. <https://doi.org/10.1088/1748-9326/aaa9c4>.
- Suhrhoff, Tim Jesper. 2022. "Phytoprevention of Heavy Metal Contamination From Terrestrial Enhanced Weathering: Can Plants Save the Day?" *Frontiers in Climate* 3. <https://www.frontiersin.org/articles/10.3389/fclim.2021.820204>.
- Suyker, Andrew E., and Shashi B. Verma. 2012. "Gross Primary Production and Ecosystem Respiration of Irrigated and Rainfed Maize–Soybean Cropping Systems over 8 Years." *Agricultural and Forest Meteorology* 165 (November): 12–24. <https://doi.org/10.1016/j.agrformet.2012.05.021>.
- Tan, Raymond R., and Kathleen B. Aviso. 2021. "On Life-Cycle Sustainability Optimization of Enhanced Weathering Systems." *Journal of Cleaner Production* 289 (March): 125836. <https://doi.org/10.1016/j.jclepro.2021.125836>.
- US Department of Commerce, NOAA. n.d. "Global Monitoring Laboratory - Carbon Cycle Greenhouse Gases." Accessed May 4, 2023. <https://gml.noaa.gov/ccgg/trends/>.
- US EPA, OAR. 2015. "Sources of Greenhouse Gas Emissions." Overviews and Factsheets. December 29, 2015. <https://www.epa.gov/ghgemissions/sources-greenhouse-gas-emissions>.
- Val Martin, Maria, Elena Blanc-Betes, Ka Ming Fung, Euripides P. Kantzas, Ilsa B. Kantola, Isabella Chiaravalloti, Lyla T. Taylor, et al. 2023. "Improving Nitrogen Cycling in a Land Surface Model (CLM5) to Quantify Soil N₂O, NO and NH₃ Emissions from Enhanced Rock Weathering with Croplands." *Geoscientific Model Development Discussions*, March, 1–32. <https://doi.org/10.5194/gmd-2023-47>.
- Verbruggen, Erik, Eric Struyf, and Sara Vicca. 2021. "Can Arbuscular Mycorrhizal Fungi Speed up Carbon Sequestration by Enhanced Weathering?" *PLANTS, PEOPLE, PLANET* 3 (5): 445–53. <https://doi.org/10.1002/ppp3.10179>.
- Vicca, Sara, Daniel S. Goll, Mathilde Hagens, Jens Hartmann, Ivan A. Janssens, Anna Neubeck, Josep Peñuelas, et al. 2022. "Is the Climate Change Mitigation Effect of Enhanced Silicate Weathering Governed by Biological Processes?" *Global Change Biology* 28 (3): 711–26. <https://doi.org/10.1111/gcb.15993>.
- Vienne, Arthur, Silvia Poblador, and Miguel Portillo-Estrada. n.d. "Frontiers | Enhanced Weathering Using Basalt Rock Powder: Carbon Sequestration, Co-Benefits and Risks in a Mesocosm Study With Solanum Tuberosum." Accessed May 4, 2023. <https://www.frontiersin.org/articles/10.3389/fclim.2022.869456/full>.
- West, Landis Jared, Steven A. Banwart, Maria Val Martin, Euripides Kantzas, and David J. Beerling. 2023. "Making Mistakes in Estimating the CO₂ Sequestration Potential of UK Croplands with Enhanced Weathering." *Applied Geochemistry* 151 (April): 105591. <https://doi.org/10.1016/j.apgeochem.2023.105591>.
- West, Tristram O., and Gregg Marland. 2002. "A Synthesis of Carbon Sequestration, Carbon Emissions, and Net Carbon Flux in Agriculture: Comparing Tillage Practices in the United States." *Agriculture, Ecosystems & Environment* 91 (1): 217–32. [https://doi.org/10.1016/S0167-8809\(01\)00233-X](https://doi.org/10.1016/S0167-8809(01)00233-X).
- West, Tristram O., and Allen C. McBride. 2005. "The Contribution of Agricultural Lime to Carbon Dioxide Emissions in the United States: Dissolution, Transport, and Net Emissions." *Agriculture, Ecosystems & Environment* 108 (2): 145–54. <https://doi.org/10.1016/j.agee.2005.01.002>.

- Wild, Bastien, Ruben Gerrits, and Steeve Bonneville. 2022. "The Contribution of Living Organisms to Rock Weathering in the Critical Zone." *Npj Materials Degradation* 6 (1): 1–16.
<https://doi.org/10.1038/s41529-022-00312-7>.
- Wild, Bastien, Gwenaël Imfeld, and Damien Daval. 2021. "Direct Measurement of Fungal Contribution to Silicate Weathering Rates in Soil." *Geology* 49 (9): 1055–58.
<https://doi.org/10.1130/G48706.1>.
- Zeri, Marcelo, Kristina Anderson-Teixeira, George Hickman, Michael Masters, Evan DeLucia, and Carl J. Bernacchi. 2011. "Carbon Exchange by Establishing Biofuel Crops in Central Illinois." *Agriculture, Ecosystems & Environment* 144 (1): 319–29.
<https://doi.org/10.1016/j.agee.2011.09.006>.
- Zhan, Ming, Adam J. Liska, Anthony L. Nguy-Robertson, Andrew E. Suyker, Matthew P. Pelton, and Haishun Yang. 2019. "Modeled and Measured Ecosystem Respiration in Maize–Soybean Systems Over 10 Years." *Agronomy Journal* 111 (1): 49–58.
<https://doi.org/10.2134/agronj2018.02.0086>.
- Zhang, Shuang, Noah J. Planavsky, Joachim Katchinoff, Peter A. Raymond, Yoshiki Kanzaki, Tom Reershemius, and Christopher T. Reinhard. 2022. "River Chemistry Constraints on the Carbon Capture Potential of Surficial Enhanced Rock Weathering." *Limnology and Oceanography* 67 (S2): S148–57. <https://doi.org/10.1002/lno.12244>.
- Zhou, Wang, Kaiyu Guan, Bin Peng, Jinyun Tang, Zhenong Jin, Chongya Jiang, Robert Grant, and Symon Mezbahuddin. 2021. "Quantifying Carbon Budget, Crop Yields and Their Responses to Environmental Variability Using the Ecosys Model for U.S. Midwestern Agroecosystems." *Agricultural and Forest Meteorology* 307 (September): 108521.
<https://doi.org/10.1016/j.agrformet.2021.108521>.

Appendix

Additional sampling not reported

In years one and two of this study, CO₂ and CH₄ emissions in Site #5 and Site #6 were measured using a Picarro GasScouter™ G4301 Mobile Gas Concentration Analyzer.

Also in years one and two, porewaters were exacted from soil samples using microrhizons, and alkalinity titrations were performed using a Hatch Titration kit. First an Orion Star™ A121 Portable pH probe is calibrated using a 3-point calibration curve. Then, the pH of 50mL of water is measured. While being stirred using a stir bar, phenolphthalein indicator is added to the water. Then, bromocresol indicator is added. Titrant is added slowly until the sample turns bright pink. The amount of titrant added is recorded, and the final pH is measured and recorded.

In year three and going forward, water samples were collected from drainage tiles and alkalinity is measured by conducting an alkalinity titration using a Hatch Digital Titrator.

Geological history of the region

Field trials on agricultural ERW in the Midwest are specifically important because of the high proportion of agriculture in the region, and because it is particularly flat, making spreading easy.

The prevalence of farming in the region can be attributed in part to deep time history of north-central Illinois which has been inland for hundreds of millions of years. As a result, there is very little topography because it is and has been so far from active margins, leading to large swaths of flat land.

Glaciation has also played a major role in shaping the landscape. Through the Pliocene and Holocene epochs there were four glacial episodes with the most recent around 12,000 years ago. During each glaciation, till and ice marginal deposits, and outwash and glacial deposits added a layer to the Illinois strata. During interglacial episodes, river, lake, and wind slope deposits altered the geology forming soil. After the last time the glaciers melted, they filled the Mississippi and Illinois rivers with fresh water. Wind then brought fine soil particles out of the river and onto the newly exposed glacial till plains.

Grasses took root in the cool, dry conditions and would grow each summer and die back each winter. As the climate warmed and summers got hotter, drier, and longer, tallgrass prairie became the dominant landscape. With their deep and persistent root systems, and cycles of growing and dying in place, feeding the ground with organic matter, they led to some of the richest soil in the world. The major soil type is mollisols, which is very fertile, and generally results from grasslands. It is rich in organic matter and dark in color.

Looking at a map of quaternary glaciation, it appears that the rich mollisols is correlated with the region where moraines are found, which makes sense as moraines deposit soil. Iroquois county is located near an end moraine. The ridge is no longer visible, due to erosion, but the uniquely rich soil is.

Understanding the geological history informs why this region is uniquely suited to agriculture, and therefore uniquely suited to large scale deployment of ERW.

Colonial history of the region

The fertile soil is also attributed, in part, to the legacy of generations of stewardship by indigenous peoples, specifically Kickapoo, Peoria, Miami, Kaskia, and Ocethi Sakowin tribes, prior to settler colonialism. Indigenous agricultural practices were diverse and included cultivating grains, beans, and fruits, especially squash, promoting tree growth to harvest nuts and seeds, and foraging native species. Large-scale agriculture arose after colonization, and then industrialization.

In the 18th-19th century, indigenous tribes resisted European American settlers who used violence and manipulation to gain control and claim ownership over the land that they had lived in interdependent relationship with for generations.

The Kickapoo and Miami tribes were involved in several large-scale multi tribal resistance movements, including Tecumseh's War from 1810-1813, where many tribes in the Great Lakes region united against the white American settlers. They were ultimately defeated by the American military force, and the tribes' confederacy dissolved.

Over the course of the following decades, tribes were continuously forced out of this region. Today, the Kickapoo nation has thousands of enrolled members in communities in Kansas, Texas, and Oklahoma. The Peoria tribe resides in Oklahoma, Miami people live in Oklahoma and Indiana primarily.

Carbon Budget

Source	Quantity	Corn (gCe m ⁻²)	uncertainty	avg (gCe m ⁻²) Soy	uncertainty	avg (gCe m ⁻²)
Internal Fluxes						
Eichemann	Re	1223.0				
Dold	Re	967.0				
Buysee	Re	930.0				
Suyker 2012		1181.0	52.8		809.0	40.7
Zhan 2019		1200.0	94.0		1000.0	120.0
<i>avg</i>				1075.3		904.5
Eichemann	GPP	-1374.0	59.0			
Dold	GPP	-1305.0			-630.0	
Buysee	GPP	-1530.0				
Moore	GPP	-1725.0	38.4		-1388.0	5.1
Dold 2019	GPP	-1483.0	100.0		-811.0	53.0
Suyker	GPP	-1536.0	74.0		-894.0	8.0
<i>avg</i>				-1492.2		-930.8
Eichemann	Harvest	393	44.0			
Dold	Harvest	492.0	42.0		182.0	12.0
Buysee	Harvest	770.0	90.0			
USDA	Harvest	561.4				
Zhan 2019					185.3	
<i>avg</i>				607.8		183.6
External Fluxes - Machinery						
Lal 2004	Harvesting (combine)	1.0		1.0	1.0	1.0
Lal 2004, We	Standard Tandem D	1.4	0.2	1.4	0.0	0.2
Lal 2004	Field cultivated (6)	0.8	0.5	0.8	0.0	0.5
Lal 2004	Seed production (9)	2.2		2.2	2.2	2.2
Lal 2004	Spray Herbicide(6)	0.1	0.1	0.1	0.1	0.1
Lal 2004	Spread fertilizer(6)	0.8	0.2	0.8	0.0	0.2
Lal 2004	Spray fertilizer(6)	0.1	0.0	0.1	0.0	0.0
Lal 2004	plant/sow/drill(6)	0.3	0.1	0.3	0.0	0.1
Lal 2004	knife-down ammoni	1.0		1.0	0.0	0.0
External Fluxes - Inputs						
Kool 2012	Herbicides	see sheet 4		11.0		18.0
Audsley et a	Fertilizer	see sheet 4		95.0		0.0
External Fluxes - Basalt						
	Mining	4.4		4.4		N/A
	Crushing	9.9				N/A
	Shipping, Diesel	26.7		26.7		N/A
	Shipping, Rail					N/A
	Shipping, EV	70.1				N/A
	Spreading	0.0		0.0		N/A
	ERW	-136.4		-136.4		N/A
Toal				199.4		179.1

Figure 25: Carbon budget for conventional/corn soy rotation

Management History of Site #2																
Quantity	Unit	Area (m ²)	Density (kg/g)	App rate (kg/m ²)	Description	Type	Form	Crop	Season	Invoice Date	Year	CO2 e. q per t Source	Notes	kg CE per m ²	kg CE per acre	kg CE per hectare
17.10	Ton	441107.74		3.52E-02	28-0-0			Corn	Spring	6-Jul	2022	2.36 Koolet al. (2014) West 2002	(2.74-12.75)	2.3E-02	93.9	232.0
1942.00	Gal	441107.74	3.79	1.67E-02	Water	Water	Liquid	Corn	Summer	10-Jun	2022		?	0.0E+00	0.0	0.0
52.00	Gal	441107.74	4.54	5.35E-04	Amsol	Water condit	Liquid	Corn	Summer	10-Jun	2022	23.1 Lal(2004); Cl 7 liquid ammi		3.4E-03	13.6	33.7
28.60	Gal	441107.74	4.13	2.68E-04	Acuron Flex II	Herbicide	Liquid	Corn	Summer	10-Jun	2022	13.9 Audsley et al. used Aatrex v		1.0E-03	4.1	10.1
26.00	Gal	441107.74	4.18	2.46E-04	Atrazine	Herbicide	Liquid	Corn	Summer	10-Jun	2022	13.90		9.3E-04	3.8	9.3
26.00	Gal	441107.74	3.23	1.90E-04	Buccaneer	Herbicide	Liquid	Corn	Summer	10-Jun	2022	18.06 Audsley et al. Used glyphos		9.4E-04	3.8	9.4
4.06	Gal	441107.74	3.48	3.21E-05	Dyne-Amic h	Surfactant	Liquid	Corn	Summer	10-Jun	2022	4.41 increases roo		3.9E-05	0.2	0.4
														0.0E+00	0.0	0.0
11.60	Ton	428967.16		2.45E-02	28-0-0	Fertilizer	Liquid	Corn	Spring	17-May	2022	6.04 Koolet al. (2014) West 2002	(2.74-12.75)	4.0E-02	163.5	403.9
20.40	Gal	428967.16	4.25	2.02E-04	Instinct 2	N stabilizer	Liquid	Corn	Spring	17-May	2022	10.00	?	5.5E-04	2.2	5.5
29.92	Gal	428967.16	4.13	2.88E-04	Acuron Flex II	Herbicide	Liquid	Corn	Spring	17-May	2022	13.90 Audsley et al. (2009); Easte		1.1E-03	4.4	10.9
27.20	Gal	428967.16	3.79	2.40E-04	Simazine	Herbicide	Liquid	Corn	Spring	17-May	2022	13.90 used simazine		9.1E-04	3.7	9.1
0.85	Gal	428967.16	4.35	8.63E-06	Sharpen	Herbicide	Liquid	Corn	Spring	17-May	2022	18.06	?	4.2E-05	0.2	0.4
27.20	Gal	428967.16	3.23	2.05E-04	Buccaneer	Herbicide	Liquid	Corn	Spring	17-May	2022	33.55 Audsley et al. (2009); Greei		1.9E-03	7.6	18.7
13.60	Gal	428967.16	3.67	1.16E-04	Fire Zone	Herbicide	Liquid	Corn	Spring	17-May	2022	5.00	?	1.6E-04	0.6	1.6
														0.0E+00	0.0	0.0
10.79	Ton	428967.16		2.28E-02	18-46-0 gran	Fertilizer	Dry	Corn	Fall	8-Nov	2021	3.36 Koolet al. (2014) West 2002	(1.66-4.19)	2.1E-02	84.6	209.0
10.79	Ton	428967.16		2.28E-02	0-0-60	Fertilizer	Dry	Corn	Fall	8-Nov	2021	0.56 Koolet al. (2014) West 2002	(0.39-0.71)	3.5E-03	14.1	34.8
5.39	Ton	428967.16		1.14E-02	21-0-0-24S	Fertilizer	Dry	Corn	Fall	8-Nov	2021	2.40	(0.75-4.67)	7.5E-03	30.2	74.6
1970.00	Gal	428967.16	3.79	1.74E-02	Water	Water	Liquid	Soy	Summer	25-Jun	2021					
17.69	Gal	428967.16	4.13	1.70E-04	dual Magnun	Herbicide	Liquid	Soy	Summer	25-Jun	2021	20.17 Lal(2004); Clements 1995		9.4E-04	3.8	9.4
29.93	Gal	428967.16	4.00	2.79E-04	Interline	Herbicide	Liquid	Soy	Summer	25-Jun	2021	23.1 Lal(2004); Clements 1995		1.8E-03	7.1	17.6
26.60	Gal	428967.16	4.52	2.80E-04	Enlist	Herbicide	Liquid	Soy	Summer	25-Jun	2021	33.55 Audsley et al. (2009); Greei		2.6E-03	10.4	25.6
79.80	Gal	428967.16	4.54	8.44E-04	Amsol	Herbicide	Liquid	Soy	Summer	25-Jun	2021	23.1 Lal(2004); Clements 1995		5.3E-03	21.5	53.1
3.99	Gal	428967.16	3.48	3.24E-05	Locktite	Surfactant	Liquid	Soy	Summer	25-Jun	2021	10		8.8E-05	0.4	0.9
2160.00	Gal	428967.16			Water	Water	Liquid	Soy	Summer	3-Jun	2021					
27.00	Gal	428967.16	4.09	2.57E-04	Boundary	Herbicide	Liquid	Soy	Summer	3-Jun	2021	20.17		1.4E-03	5.7	14.1
10.13	Gal	428967.16	3.48	8.22E-05	Griptite	Surfactant	Liquid	Soy	Summer	3-Jun	2021	10	methyalted s	2.2E-04	0.9	2.2
27.00	Gal	428967.16	3.23	2.03E-04	Buccaneer	Herbicide	Liquid	Soy	Summer	3-Jun	2021	18.06 Audsley et al. Used glyphos		1.0E-03	4.1	10.0
27.00	Gal	428967.16	4.36	2.74E-04	Salvan	Herbicide	Liquid	Soy	Summer	3-Jun	2021	18.06	2,4-D, used gl	1.4E-03	5.5	13.5
54.00	Gal	428967.16	4.54	5.71E-04	Amsol	Herbicide	Liquid	Soy	Summer	3-Jun	2021	23.1		3.6E-03	14.6	36.0
1435.70	Gal	428967.16			Water	Water	Liquid	Corn	Winter	7-Dec	2020					
50.20	Gal	428967.16	4.54		Amsol	Herbicide	Liquid	Corn	Winter	7-Dec	2020	20.17 Lal(2004); Clements 1995				
33.00	Ozs	428967.16			Autumn Supe	Herbicide	Liquid	Corn	Winter	7-Dec	2020					
27.31	Gal	428967.16			Brash Bulk	Herbicide	Liquid	Corn	Winter	7-Dec	2020					
7.97	Ton	428967.16			18-46-0	Fertilizer	Dry	Corn	Fall	31-Oct	2020					
7.97	Ton	428967.16			0-0-60	Fertilizer	Dry	Corn	Fall	31-Oct	2020					
19.00	Ton	437060.88			28-0-0	Fertilizer	Sidedress(liq)	Corn	Summer	11-Aug	2020					
2052.00	Gal	437060.88			Water	Water	Liquid	Corn	Summer	11-Aug	2020					
54.84	Gal	437060.88	4.54		Amsol	Herbicide	Liquid	Corn	Summer	11-Aug	2020					
27.00	Gal	437060.88	4.18		Atrazine 4L IV	Herbicide	Liquid	Corn	Summer	11-Aug	2020					
27.00	Gal	437060.88	4.13		Acuron Flex II	Herbicide	Liquid	Corn	Summer	11-Aug	2020					
5.06	Gal	437060.88			Locktite	Surfactant	Liquid	Corn	Summer	11-Aug	2020					
324.00	Oz	437060.88			Status	Herbicide	Liquid	Corn	Summer	11-Aug	2020					
11.94	Ton	441107.74			29-0-0-4S	Fertilizer	Liquid	Corn	Summer	31-Jul	2020					
436.00	Gal	441107.74			Water	Water	Liquid	Corn	Summer	31-Jul	2020					
26.25	Gal	441107.74	4.18		Atrazine 4L Bi	Herbicide	Liquid	Corn	Summer	31-Jul	2020					
29.98	Gal	441107.74	4.13		Acuron	Herbicide	Liquid	Corn	Summer	31-Jul	2020					
27.25	Gal	441107.74			Honcho H6 G	Herbicide	Liquid	Corn	Summer	31-Jul	2020					
10.22	Gal	441107.74			Grptite MSO	Surfactant	Liquid	Corn	Summer	31-Jul	2020					
5.11	Gal	441107.74			Diflexx	Herbicide	Liquid	Corn	Summer	31-Jul	2020					
3.41	Gal	441107.74			Agrotain	N stabilizer	Liquid	Corn	Summer	31-Jul	2020					

Figure 26: Management history of Site #2. Sites #1 and #3 received similar treatment.

Pioneer Valley Basalt Particle Size and Mineralogy

Particle Size Distribution Report			
Sieve Size	Weight	% Passing	Spec. % Retained
2"	0	100.0	0.0
1 1/2"	0	100.0	0.0
1"	0	100.0	0.0
3/4"	0	100.0	0.0
1/2"	0	100.0	0.0
3/8"	0	100.0	0.0
1/4"	0	100.0	0.0
# 4	0.2	100.0	0.0
# 8	6.5	99.1	0.9
# 10	2.2	98.8	1.2
# 16	7.9	97.7	2.3
# 30	28.3	93.7	6.3
# 40	33.6	89.0	11.0
# 50	54.1	81.4	18.6
# 60	32.6	76.9	23.1
# 100	110.9	61.4	38.6
# 200	163.6	38.5	61.5
Pan	275.9		
Total	715.80		
Material Type:	Float		
Source:	Plant # 1		
Sampled By:	MWM		
Test By:	DCT		
Comments:	Fisher Air Classifier by product		
NETTCP Certification #	170		

Figure 27: Pioneer Valley Basalt Particle Size Distribution (provided by Rock Dust Local)



Analytical Report



Rock Dust Local LLC
 1445 Hemenway Rd.
 Bridport, Vermont 05734
 802-758-2220
www.RockDustLocal.com

Report ID: AgReport- A14-00203

Sample Name: Pioneer Valley Basalt

Report Date: 1/31/2014

Analysis Methods

1) FUS-ICP (Fusion-Inductively Coupled Plasma)

An oxidized sample is dissolved in a borate flux and then diluted in aqueous nitric acid. ICP-OES is used to quantify various elements in the resulting solution.

2) TD-ICP (Total Digestion-Inductively Coupled Plasma)

A sample is digested via sequential addition of hydrofluoric, perchloric, and nitric acids. The acids are evaporated and the residue reconstituted in aqua regia. ICP-OES is used to quantify various elements in the resulting solution.

3) INAA (Instrumental Neutron Activation Analysis)

Samples are bombarded with neutrons to generate radioactive nuclides. Measurement of the energy and intensity of the alpha particles generated by their subsequent decay is used to quantify the various elements present in the original sample.

4) PGNAA (Prompt Gamma Neutron Activation Analysis)

Similar to INAA, except the energy and intensity of the alpha particles generated during neutron bombardment is used to quantify the various elements present in the original sample.

5) TD-MS (Total Digestion-Inductively Coupled Plasma -Mass Spectrometry)

A sample is digested via sequential addition of hydrofluoric, perchloric, and nitric acids. The acids are evaporated and the residue reconstituted in aqua regia. ICP-MS is used to quantify various elements in the resulting solution.

6) Satmagan

The force acting in a sample is measured while it is in a magnetic field with a spatial gradient.

	Test Value	Unit Symbol	Detection Limit	Analysis Method
Silicon dioxide (SiO2)	51.62	%	0.01	FUS-ICP
Aluminium oxide (Al2O3)	13.64	%	0.01	FUS-ICP
Iron oxide (Fe2O3(T))	13.16	%	0.01	FUS-ICP
Manganese oxide (MnO)	0.20	%	0.01	FUS-ICP
Magnesium oxide (MgO)	5.77	%	0.01	FUS-ICP
Calcium oxide (CaO)	9.15	%	0.01	FUS-ICP
Sodium oxide (Na2O)	2.98	%	0.01	FUS-ICP
Potassium oxide (K2O)	0.87	%	0.01	FUS-ICP
Titanium dioxide (TiO2)	0.978	%	0.005	FUS-ICP
Phosphorus pentoxide (P2O5)	0.13	%	0.01	FUS-ICP
Loss on Ignition (LOI)	2.29	%		FUS-ICP
Total	100.80	%	0.01	FUS-ICP
Gold (Au)	< 5	ppb	5	INAA
Silver (Ag)	< 0.5	ppm	0.5	2 / 3
Arsenic (As)	4	ppm	2	INAA
Barium (Ba)	146	ppm	3	1 / 3
Beryllium (Be)	< 1	ppm	1	FUS-ICP
Bismuth (Bi)	< 2	ppm	2	TD-ICP
Bromine (Br)	< 1	ppm	1	INAA
Cadmium (Cd)	< 0.5	ppm	0.5	TD-ICP
Cobalt (Co)	51	ppm	1	INAA
Chromium (Cr)	24	ppm	1	INAA
Cesium (Cs)	< 0.5	ppm	0.5	INAA
Copper (Cu)	67	ppm	1	TD-ICP
Hafnium (Hf)	2.3	ppm	0.5	INAA
Mercury (Hg)	< 1	ppm	1	INAA
Iridium (Ir)	< 5	ppb	5	INAA
Molybdenum (Mo)*	0.6*	ppm	0.1	TD-MS
Nickel (Ni)	36	ppm	1	TD-ICP
Lead (Pb)	< 5	ppm	5	TD-ICP
Rubidium (Rb)	< 20	ppm	20	INAA
Sulfur (S)	0.082	%	0.001	TD-ICP
Antimony (Sb)	< 0.2	ppm	0.2	INAA
Scandium (Sc)	42.3	ppm	0.1	INAA
Selenium (Se)	< 3	ppm	3	INAA
Strontium (Sr)	168	ppm	2	FUS-ICP
Tantalum (Ta)	< 1	ppm	1	INAA
Thorium (Th)	3.0	ppm	0.5	INAA
Uranium (U)	< 0.5	ppm	0.5	INAA
Vanadium (V)	349	ppm	5	FUS-ICP
Tungsten (W)	< 3	ppm	3	INAA
Yttrium (Y)	29	ppm	1	FUS-ICP
Zinc (Zn)	94	ppm	1	TD-ICP
Zirconium (Zr)	79	ppm	2	FUS-ICP
Lanthanum (La)	10.0	ppm	0.2	INAA
Cerium (Ce)	30	ppm	3	INAA
Neodymium (Nd)	10	ppm	5	INAA
Samarium (Sm)	2.7	ppm	0.1	INAA
Europium (Eu)	0.8	ppm	0.1	INAA
Terbium (Tb)	< 0.5	ppm	0.5	INAA
Ytterbium (Yb)	2.5	ppm	0.1	INAA
Lutetium (Lu)	0.42	ppm	0.05	INAA
Mass	1.347	g		INAA
Boron (B)	279	ppm	2	PGNAA
Mass	1.080	g		PGNAA
% Magnetite	1.8	%	0.1	Satmagan

*Result reported from Report A11-2798

This report shall not be reproduced without the consent of Activation Laboratories.
 Analytical results pertain only to those sample(s) received by the laboratory.
 Your personal information is managed according to the Privacy Act. We will not willfully disclose individually identifiable information.

Results Approved By:

Steve Jenkins
 Steve Jenkins, PhD

Activation Laboratories - Agriculture Division • 1480 Sandhill Drive, Unit 9, Ancaster, ON L9G 4V5 • 289.204.0515 • laboratory@actlabs.com

Figure 28: Pioneer Valley Basalt Mineralogy (provided by Actlabs via Rock Dust Local)